Int J Earth Sci (Geol Rundsch) (2013) 102:1111–1129
DOI 10.1007/s00531-012-0845-5

ORIGINAL PAPER

Paleoenvironmental conditions and strontium isotope stratigraphy in the Paleogene Gafsa Basin (Tunisia) deduced from geochemical analyses of phosphatic fossils

László Kocsis · Anouar Ounis · Fredj Chaabani · Neili Mohamed Salah

Received: 24 August 2012 / Accepted: 10 November 2012 / Published online: 13 December 2012

Abstract Fossil shark teeth and coprolites from three major phosphorite occurrences in the Gafsa Basin (southwestern Tunisia) were investigated for their geochemical compositions to improve local stratigraphy and to better assess paleoenvironmental conditions. $^{87}Sr/^{86}Sr$ isotope ratios of shark teeth from the Early Maastrichtian El Haria Formation and from the Early Eocene Métlaoui *s.s.* Formation yielded Sr isotope ages of 68 ± 1 and 47.9 ± 1.3 Ma, respectively, which accord with the expected stratigraphic positions of these sediments. Conversely, shark teeth from the Paleocene–Eocene Chouabine Formation have large variation in Sr isotope ratios even within individual layers. After statistical treatment and then elimination of certain outlier samples, three age-models are proposed and discussed. The most reasonable solution includes three subsequent Sr ages of 61.8 ± 2.2 Ma, 57.2 ± 1.8 and 54.6 ± 1.6 for layer IX, layers VIII–V and layers IV–0, respectively. Three scenarios are discussed for explanation of the presence of the outliers: (1) diagenesis, (2) re-working and (3) locally controlled seawater Sr isotope ratio. The most plausible account for the higher $^{87}Sr/^{86}Sr$ ratios relative to the global ocean in some fossils is enhanced intrabasinal re-working due to low sea level. Conversely, the sample with lower $^{87}Sr/^{86}Sr$ than the global seawater may link to diagenesis or to seawater influenced by weathering of Late Cretaceous marine carbonates, which latter is supported by model calculation as well. The ε_{Nd} values of these fossils are very similar to those reported for Paleogene and Late Cretaceous Tethyan seawater and are compatible with the above interpretations. The relatively low oxygen isotope values in shark teeth from the topmost phosphate bed of the Chouabine Formation, together with the Sr isotope results, point toward recovering better connections with the open sea. These $\delta^{18}O$ data reflect elevated ambient temperature, which may link to the Early Eocene Climatic Optimum.

Keywords Paleocene–Eocene · Strontium isotope stratigraphy · Oxygen isotope · Phosphate · Shark teeth · Tunisia

L. Kocsis (✉)
UNIL-GEOPOLIS, Institute of Earth Sciences,
Université de Lausanne, 1015 Lausanne, Switzerland
e-mail: laszlo.kocsis@unil.ch

A. Ounis · F. Chaabani
Laboratoire des Ressources Minérales et Environnement
Faculté des Sciences de Tunis, Université de Tunis El Manar,
Tunis, Tunisia

N. M. Salah
Direction de Géologie, Compagnie des Phosphates
de Gafsa, Métlaoui, Tunisia

Introduction

The paleoenvironmental and paleodepositional conditions of phosphorite beds in the Late Cretaceous–Early Paleogene Gafsa Basin (Fig. 1) were described by Ounis et al. (2008) using stable isotope and rare earth element (REE) chemistry of phosphatic fossils. REE compositions of shark teeth and coprolites have revealed suboxic–anoxic depositional conditions in the Early Maastrichtian, while the environment was rather oxic–suboxic in the Upper Paleocene–Eocene. Carbon isotope compositions in the Paleogene fossils yielded low $\delta^{13}C$ values with a pronounced negative carbon isotope excursion (CIE) in the upper part of the Chouabine Formation (Ounis et al. 2008; Fig. 2). This was recognized in two different localities (Fig. 1; Bliji

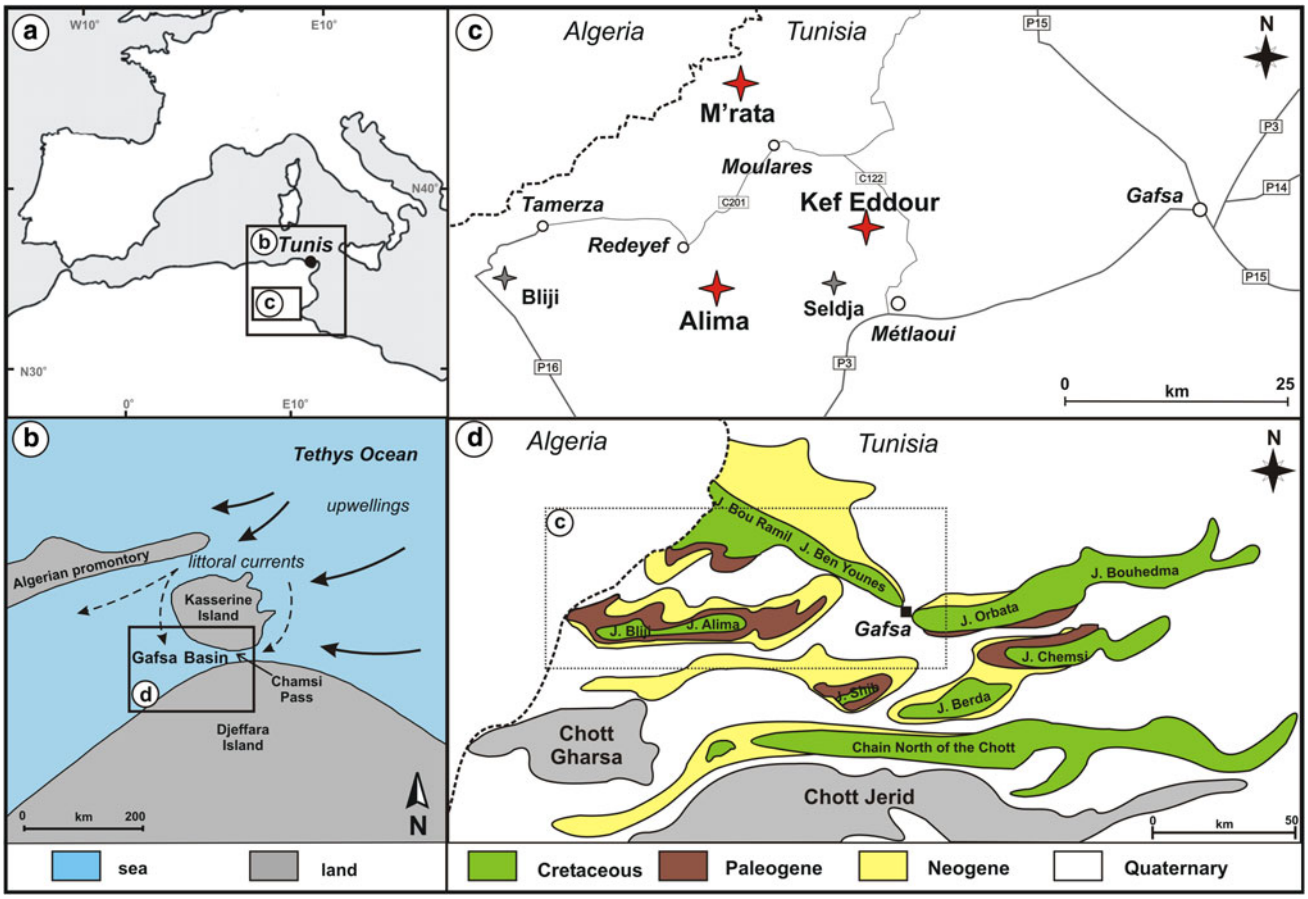

Fig. 1 **a** Geographic position of the studied area in Tunisia. **b** General paleogeographic situation of the Gafsa Basin from the Maastrichtian to Early Eocene (Sassi 1974; Burollet and Oudin 1980; Chaabani 1995; Zaïer et al. 1998); *arrows* indicate potential upwelling and littoral currents from the Tethys Ocean. **c** The position of the sampled localities and sections in the Gafsa Basin; *red stars*—new data provided in this study; *gray stars*—geological sections described in literature: Seldja (Bolle et al. 1999; Adatte et al. 2002); Bliji Mountain (Ounis et al. 2008); Oum El Khecheb (Galfati et al. 2010). **d** Simplified geological map of the region after Ragaya et al. (1991)

and Alima Mountains) and registered with both types of fossils (shark teeth and coprolites). Therefore, the observed CIE was proposed as a possible reflection of the negative $\delta^{13}C$ anomaly documented at the Paleocene–Eocene boundary (e.g., Aubry et al. 1996; Bains et al. 1999; Zachos et al. 2001). The $\delta^{13}C$ values in some cases, however, are exceptionally low; hence, they could relate to enhanced organic matter recycling too. The globally known negative CIE is also accompanied by extreme warm climate, the so called Paleocene–Eocene Thermal Maximum (PETM), which can be traced by oxygen isotope composition of marine fossils (e.g., Kennett and Stott 1991; Thomas et al. 1999; Sluijs et al. 2006). Oxygen isotope compositions of the fossils from the Gafsa Basin were found compatible with stable warm climatic conditions; however, they do not show any exceptional surplus warming during the Paleogene. This was explained by the tropical climate and semi-closed paleogeographic situation of the Gafsa Basin during this period (Ounis et al. 2008).

To confirm the validity of the link between the CIE and Paleocene–Eocene transition (P/E) in the Gafsa Basin by biostratigraphy is difficult. This is due to phosphatization/dissolution of microfossils, especially the calcareous ones. Occasionally, these fossils are preserved in intercalated marl or carbonate beds, but generally, they do not have real biostratigraphic value. Reworking processes and possible mixing between layers by active bioturbation make biostratigraphic work further complicated. The exact position of the P/E therefore is not accurately known, and discrepancies referring to the age of the main phosphate series are apparent in the literature (Ben Abdessalam 1978; Chaabani 1995; Bolle et al. 1999; Henchiri 2007; Ben Hassen et al. 2010; Galfati et al. 2010; Zili 2010).

As next step to improve stratigraphy and our understanding about the paleoenvironmental conditions during the deposition of these phosphorite beds, we present strontium isotope data from biogenic apatite with the aim to assess Sr isotope stratigraphy. Additionally, few samples

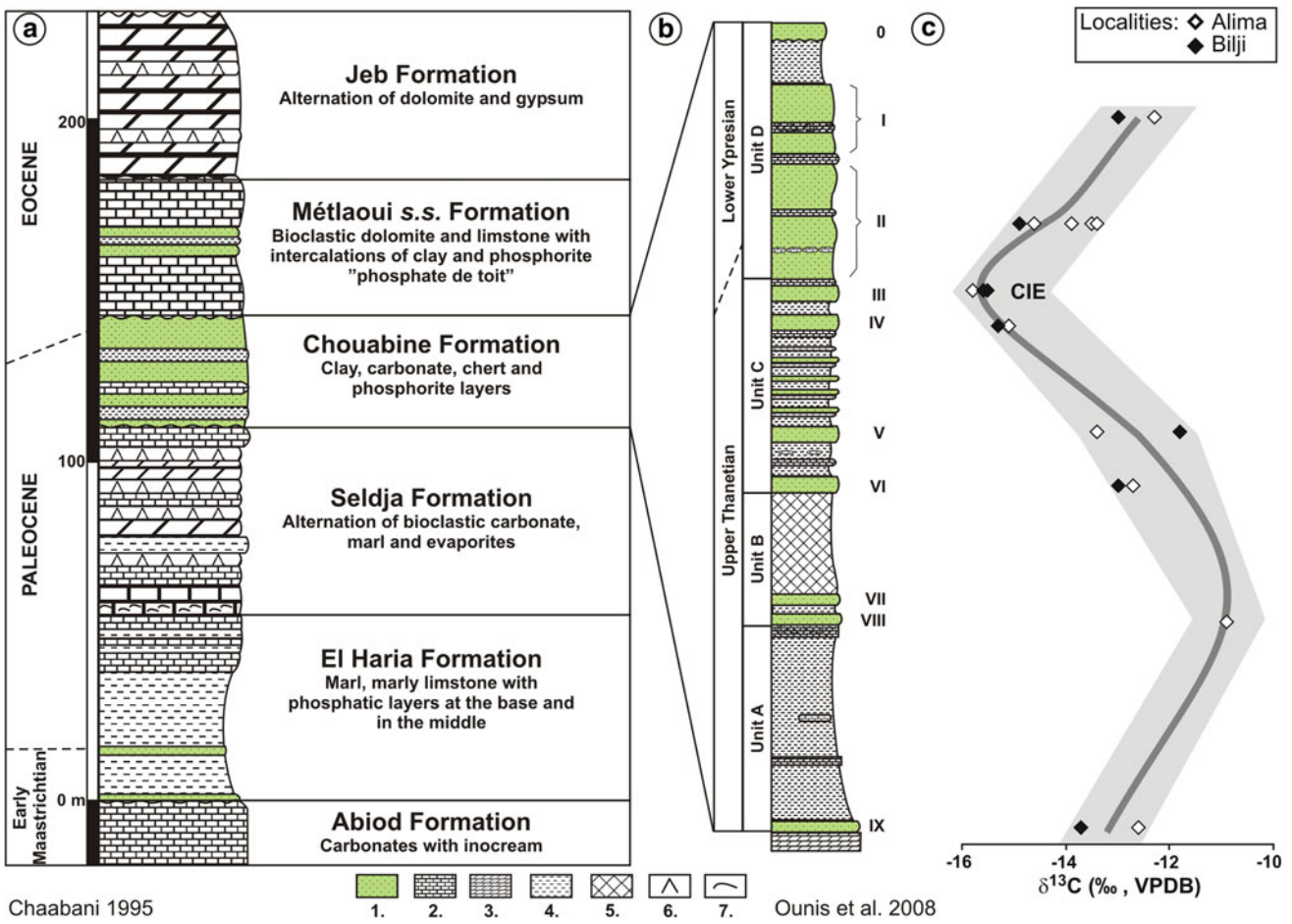

Fig. 2 **a** General stratigraphic scheme of the Upper Cretaceous–Eocene marine sedimentary sequences in the Gafsa Basin after Chaabani (1995). The studied phosphate beds are in the El Haria, Chouabine and Métlaoui *s.s.* Formations. Note that in other division the Seldja, Chouabine and Métlaoui *s.s.* Formations appear as sub-members of the Métlaoui Group (e.g., Zaïer et al. 1998; Galfati et al. 2010). **b** The principal phosphate layers of the Chouabine Formation with four sub-units (*A–D*) and the ten major phosphate layers (IX–0); legends: 1—phosphate; 2—limestone; 3—dolomite; 4—marl; 5—chert; 6—evaporite; 7—lumachelle. **c** Carbon isotope composition of coprolites after Ounis et al. (2008) showing a negative shift in the top of unit-C of the Chouabine Formation that was related to the Paleocene–Eocene boundary

were also analyzed for neodymium and oxygen isotope compositions, and they are discussed along with the Sr isotope data.

Geochemical background

The variation of $^{87}Sr/^{86}Sr$ in seawater is the results of the relative amounts and the isotopic compositions of different sources (e.g., continental run off, mid-ocean ridge volcanism) that contribute Sr into the oceans (e.g., Frank 2002). The residence time of Sr in seawater is in the range of 10^6 years, several orders of magnitude longer than oceanic mixing time (Frank 2002). The oceans are therefore well mixed with respect to Sr. As a consequence, the $^{87}Sr/^{86}Sr$ ratio of the global ocean remains relatively stable with time; thus, the temporal variation in the Sr isotope ratio of seawater enables geological dating of sedimentary materials deposited within marine environment (Burke et al. 1982; Koepnick et al. 1985; Hodell et al. 1991; Ingram 1995; Barrat et al. 2000).

McArthur et al. (2001) established a reference curve for the global variation of Sr isotope ratio in seawater for the Phanerozoic. This curve is supported by a look-up table and provides numerical ages with 95 % confidence limit for a certain $^{87}Sr/^{86}Sr$ ratio; therefore, it is often used to date marine sediments. The data used for creating the curve come from well-dated localities (e.g., available radiometric ages, detailed magnetostratigraphy or well-constrained biostratigraphy) and from well-preserved marine samples because diagenetic alteration can be a major issue (McArthur and Howarth 2004). Owing to the well-constrained scheme of the McArthur database, our results from the Gafsa Basin are largely compared to their curve in this paper, however, it must be mentioned that another important marine Sr-isotope

compilation exists (Veizer et al. 1999, then updated by Prokoph et al. 2008). This essentially shows the same Sr isotope trend and changes through time pointing to the robustness of the Sr isotope dating. These authors, however, do not add statistical smoothing to their database; hence, their compilation reveals certain variations and obvious outliers around the general trend. These latter can be related to diagenesis and possibly inaccurate stratigraphy, or might reflect some real variations at a given time.

Contrary to $^{87}Sr/^{86}Sr$, the Nd isotope ratio in seawater is heterogeneous due to its much lower concentration and its shorter residence time than the oceanic turnover (Arsouze et al. 2009). Hence, the Nd isotope ratio of marine sediments and fossils can help in distinguishing among different water masses, and it is widely applied in paleoceanography (Piepgras and Wasserburg 1980; Palmer and Elderfield 1985; Vance and Burton 1999; Martin and Haley 2000; Frank 2002). Although the REE contents of the phosphatic fossils are almost purely diagenetic, their Nd isotope ratios could be still linked to seawater composition (Staudigel et al. 1985; Elderfield and Pagett 1986; Stille et al. 1996; Martin and Scher 2004). Therefore, application of REE chemistry and Nd isotope ratios of fossil biogenic apatite are broadly used in characterizing paleoenvironmental conditions or tracing paleoseawater compositions (e.g., Vennemann and Hegner 1998; Thomas et al. 2003; Lécuyer et al. 2004; Scher and Martin 2006; Pucéat et al. 2005; Kocsis et al. 2009).

The oxygen isotope composition of biogenic apatite as a climate proxy is well documented (e.g., Longinelli and Nuti 1973; Kolodny et al. 1983; Kohn and Cerling 2002). The $\delta^{18}O_{PO4}$ composition in fish teeth depends on the oxygen isotope composition of seawater and water temperature at the time of their growth (e.g., Kolodny et al. 1983; Pucéat et al. 2010). Knowing the $\delta^{18}O$ of seawater, the ambient temperature can be calculated from the $\delta^{18}O_{PO4}$ values. Generally, global mean seawater oxygen isotopic composition varies between 0.5 and −1 ‰ due to global temperature and/or ice volume fluctuations between Icehouse and Greenhouse periods (e.g., Dansgaard 1964; Zachos et al. 2001). However, shallow seas or sea surface isotopic composition can be locally lowered by enhanced river input or increased by evaporation at low latitudes. Hence, getting reliable absolute temperature data is sometimes difficult and bears many uncertainties, but relative changes in the $\delta^{18}O_{PO4}$ values often give valuable information about paleoenvironmental conditions.

Local geology

In the Late Cretaceous–Early Paleogene, the southern Tethys Ocean covered most of the Tunisian landmass. Only some areas like the Djeffara and Kasserine Islands were raised. The Gafsa Basin was located between these islands (Fig. 1). Connection of this basin with the open sea was largely maintained from the west, and sometimes water exchange occurred in the east through the Chamsi corridor (Chaabani 1995). Sedimentation took place under semi-closed conditions mainly influenced by sea-level fluctuation generating inner neritic to coastal depositional environments (Sassi 1974; Chaabani 1995; Zaïer et al. 1998; Ounis et al. 2008). During this period, phosphorite formations occurred several times (Fig. 2a). The first phosphorite deposition took place on the hardgrounds of the Abiod Formation, which is Early Maastrichtian in age. The thickness of these phosphorite rich beds can locally reach one meter. This facies is overlain by thick successions of dark marls and marly limestone. All these layers belong to the El Haria Formation, which continued developing in northern Tunisia till the Early Eocene (Chaabani 1995; Bolle et al. 1999; Zaïer et al. 1998).

However, in the Gafsa Basin, euxinic and lagoonal conditions set in during the Paleocene (Seldja Formation), and later in the Thanetian–Early Ypresian, economically important phosphorites were deposited. These sediments are attributed to the Chouabine Formation (Fournier 1980). Its thickness generally varies from 40 to 100 m and consists of phosphorite beds interbedded with gray shale, thin calcareous marl and occasionally metric chert beds (Sassi 1974; Chaabani 1995). Based on sedimentological observations and, for example, on the distribution of chert layers in the Gafsa Basin, a clear decreasing water depth from west to east is indicated (Ounis 2011). Maximum water depth in the basin was about 100 m (Adatte et al. 2002). The Chouabine Formation can be subdivided into four units (A-D), where ten major phosphate layers are recognized. These are named from the base to the top as layer IX to layer 0, respectively (Fig. 2b). Close to the limit of unit-C and unit-D, between layer II and III–IV, a large negative $\delta^{13}C$ excursion was observed in phosphatic fossils (Fig. 2c), which was related to the PETM event (Ounis et al. 2008).

The Chouabine Formation is overlain by Ypresian–Lutetian carbonates, which are attributed to the Métlaoui sensu stricto Formation (Fournier 1980). In a wider sense, the name Métlaoui Formation often appears in the literature as including the Seldja and Chouabine Formations as the lower and middle members of the Métlaoui Formation Group (e.g., Zaïer et al. 1998). The Métlaoui *s.s.* Formation contains the last and the youngest phosphorite beds, which are locally called "phosphate de toit." The marine sedimentary sequence in the Gafsa Basin ends by massive gypsum and dolomitic beds of the Jebs Formation (Chaabani 1995; Zaïer et al. 1998).

The phosphorite sediments in the Gafsa Basin have been studied since the nineteenth century and have been the

target of several researches (e.g., Thomas 1885; Pervinquière 1903; Cayeux 1941; Burollet 1956; Sassi 1974; Fournier 1980; Belayouni 1983; Chaabani 1995; Keller et al. 1998; Zaïer et al. 1998; Bolle et al. 1999; Béji-Sassi 1999; Adatte et al. 2002; Ben Hassen et al. 2009, 2010; Galfati et al. 2010). Ounis et al. (2008) published the first detailed geochemical study, including stable isotope chemistry, on the phosphatic fossils from these series. As an extension of previous research on these sediments, we present radiogenic isotope ratios (strontium and neodymium) from the same samples studied by Ounis et al. (2008) from the Alima Mountain. Additional samples were collected from the phosphate layers of the Chouabine and Métlaoui *s.s.* Formations in the regions of Kef Eddour and M'rata (Fig. 1c). These new samples are mainly shark teeth, which were analyzed for strontium isotope ratio and for oxygen isotope composition.

Samples and methods

Ounis et al. (2008) gave a detailed description of the phosphatic remains from the Gafsa Basin and concluded that shark teeth are well preserved and they resemble modern teeth in their structure, major element compositions and mineralogy. Coprolites exhibit much finer structure and higher carbonate content compared to the teeth. These fossils are mineralized remains of originally organic-rich fecal pellets that derive from fish and/or crustaceans, and they were phosphatized in the sediment and/or in the sediment/water interface at the bottom of the sea. Therefore, the chemical and isotopic compositions of coprolites rather link to pore-water conditions in the early diagenetic environment, while shark teeth enameloid could provide information from the water column if they are not diagenetically altered.

Shark teeth and coprolites from the formerly studied section in the Alima Mountain (Ounis et al. 2008) were prepared for Sr and Nd isotope analyses. Six shark teeth and seven coprolites were measured for $^{87}Sr/^{86}Sr$ ratios, while five $^{143}Nd/^{144}Nd$ analyses were done: two on coprolites and three on mixed teeth and coprolites (cf. Table 1). Mixed samples were prepared on account of the small sample quantities and their relatively low Nd-content. Previous trace element study on these fossils yielded identical REE element distribution (Ounis et al. 2008); hence, the Nd isotope ratios in these fossils are assumed to be very similar.

Additionally, shark teeth (Lamniformes and within mainly the family of Odontaspididae) were collected from the phosphate layers of the Chouabine Formation in the Kef Eddour region, while shark teeth and one crocodile tooth were obtained near Métlaoui and M'rata cities from the youngest phosphate beds in the Métlaoui *s.s.* Formation (Table 2; Figs. 1, 2). From each layer, two well-preserved teeth were chosen and sampled to collect only well-crystallized and resistant enameloid.

All the samples were cleaned in an ultrasonic bath to reduce sedimentary contamination. Tooth enameloid was then sampled with a microdrill by shaving off the outer shiny enameloid layer of the teeth. Coprolites were crushed in an agate mortar. The sample powders thus obtained were pre-treated in two steps following the procedures of Koch et al. (1997). First, they were leached overnight in 2–2.5 % NaOCl to remove any residual soluble organic matter and then for 6–12 h in 1 M acetic acid-Ca-acetate buffer (pH 4.5) to remove exogenous carbonates. Samples from the Métlaoui *s.s.* Formation and from the top phosphate bed (layer 0) of the Chouabine Formation were prepared for oxygen isotope analyses following the method of O'Neil et al. (1994) and Dettman et al. (2001). The phosphate group of the biogenic apatite was separated and precipitated as Ag_3PO_4 and were measured as triplicates for each samples. The silver phosphate was converted to CO at 1,450 °C via reduction with graphite using a TC/EA (high-temperature conversion elemental analyzer) (Vennemann et al. 2002) and was measured on a Finnigan MAT Delta Plus XL mass spectrometer at the University of Lausanne. The results were corrected to Ag_3PO_4 in-house phosphate standards that normally have better than ±0.3 ‰ standards deviations during measurements. NBS-120c phosphorite rock reference material was prepared and run parallel with the samples, and a value of 21.5 ± 0.2 ‰ was obtained. Isotope compositions are expressed in the δ-notation relative to Vienna Standard Mean Ocean Water (VSMOW).

Subsamples of pre-cleaned powders were further prepared for Sr and Nd isotope analyses, which were done at the National Oceanography Centre, University of Southampton. Sr was separated using Sr-Spec columns and loading onto Ta filaments with a Ta activator solution. The Nd separation was carried out using a 2-column procedure: a cation column to remove the major elements, followed by a Ln-Spec column to separate Nd from the other REEs. The Nd samples were loaded onto the Ta sides of a Ta–Re–Ta triple-filament assembly. The $^{87}Sr/^{86}Sr$ and $^{143}Nd/^{144}Nd$ ratios were analyzed on a VG-Micromass Sector 54 Thermal Ionization Mass Spectrometer (TIMS). A multi-dynamic peak jumping procedure was used with a ^{88}Sr beam size of 2 V and ^{144}Nd beam size of 1 V.

The NIST-987 Sr and the JNdi-certified reference materials were run parallel with the samples, and they yielded values of $^{87}Sr/^{86}Sr$ ratio of 0.710249 ± 0.000020 ($n = 7$, 2σ) and $^{143}Nd/^{144}Nd$ ratio of 0.512091 ± 0.000006 ($n = 3$, 2σ), respectively. The data presented here were corrected for each run to the accepted isotopic ratios of 0.710248 (NIST 987—McArthur et al. 2001) and 0.512115

Table 1 Samples from the Gafsa Basin: (a) Alima Mountain: the same shark teeth and coprolites were used for radiogenic isotope analyses that had previously been investigated for trace element and stable isotope compositions (Ounis et al. 2008). (b) Geochemical data of the shark teeth and one crocodile tooth from Kef Eddour, M'rata and Métlaoui

Samples	Lithostratigraphy	Age	Layers	Shark teeth				Coprolites				Teeth (t) and coprolite (c)			
				Sr (ppm)	Nd (ppm)	$^{87}Sr/^{86}Sr$	2SE × 10^{-6}	Sr (ppm)	Nd (ppm)	$^{87}Sr/^{86}Sr$	2SE × 10^{-6}		$^{143}Nd/^{144}Nd$	2SE × 10^{-6}	ε^0_{Nd}
(*a*) *Alima Mountain (Gafsa Basin)—cf.* Ounis et al. (2008)															
ZT2	Chouabine Fm.	Paleocene–Eocene	Layer I	1,737	42.6	0.707804	11	1,819	51.8	0.707781	14	*c* + *t*	0.512202	6	−8.5
ZT6	Chouabine Fm.	Paleocene–Eocene	Layer II	1,576	62.8	0.707782	17	1,922	36.0	0.707769	11	*c* + *t*	0.512179	5	−9.0
ZT8	Chouabine Fm.	Paleocene–Eocene	Layer IV	1,974	30.0	0.707762	10	1,919	18.3	0.707775	10		–	–	–
ZT10	Chouabine Fm.	Paleocene–Eocene	Layer VI	–	–	–	–	2,002	21.6	0.707778	13		–	–	–
ZT11	Chouabine Fm.	Paleocene–Eocene	Layer VII–VIII	1,630	28.3	0.707786	11	1,883	20.2	0.707785	10	*c* + *t*	0.512210	8	−8.3
ZT12	Chouabine Fm.	Paleocene–Eocene	Layer IX	1,548	87.2	0.707821	11	2,110	53.4	0.707801	14	*c*	0.512113	6	−10.2
K4	El Haria Fm.	Upper Cretaceous		2,258	151.8	0.707795	11	1,932	71.2	0.707785	14	*c*	0.512175	14	−9.0

Samples	Lithostratigraphy	Age	Layers	$\delta^{18}O$ SMOW	Std.	$^{87}Sr/^{86}Sr$	2SE × 10^{-6}
(*b*) *Kef Eddour and M'rata (Gafsa Basin)*							
PTMt-1	Métlaoui Fm.	? Lutetian	Phosphate de toit—Métlaoui	20.5	0.1	0.707740	13
PTMt-3	Métlaoui Fm.	? Lutetian	Phosphate de toit—Métlaoui	19.4	0.1	0.707727	10
PTMr-1	Métlaoui Fm.	? Lutetian	Phosphate de toit—M'rata	20.4	0.1	0.707730	11
PTMr-2	Métlaoui Fm.	? Lutetian	Phosphate de toit—M'rata	19.9	0.0	0.707741	10
PTMr-3	Métlaoui Fm.	? Lutetian	Phosphate de toit—M'rata	19.7	0.2	–	–
PTMrCroc	Métlaoui Fm.	? Lutetian	Phosphate de toit—M'rata	20.5	0.1	0.707848	11[a]
0/1	Chouabine Fm.	Paleocene–Eocene	Layer 0	19.8	0.0	0.707740	11
0/2	Chouabine Fm.	Paleocene–Eocene	Layer 0	18.7	0.1	–	–
0/3	Chouabine Fm.	Paleocene–Eocene	Layer 0	19.4	0.2	–	–
0/4	Chouabine Fm.	Paleocene–Eocene	Layer 0	19.1	0.1	0.707749	11
I/3	Chouabine Fm.	Paleocene–Eocene	Layer I	–		0.707761	11
I/4	Chouabine Fm.	Paleocene–Eocene	Layer I	–		0.707763	11
II/1	Chouabine Fm.	Paleocene–Eocene	Layer II	–		0.707750	10
II/2	Chouabine Fm.	Paleocene–Eocene	Layer II	–		0.707749	11
III–IV/1	Chouabine Fm.	Paleocene–Eocene	Layer III–IV	–		0.707767	11
III–IV/2	Chouabine Fm.	Paleocene–Eocene	Layer III–IV	–		0.707749	11

Table 1 continued

Samples	Lithostratigraphy	Age	Layers	δ^{18}O SMOW	Std.	$^{87}Sr/^{86}Sr$	2SE × 10^{-6}
V/2	Chouabine Fm.	Paleocene–Eocene	Layer V	–		0.707781	11
V/3	Chouabine Fm.	Paleocene–Eocene	Layer V	–		0.707774	10
VII/1	Chouabine Fm.	Paleocene–Eocene	Layer VII	–		0.707743	14
VII/2	Chouabine Fm.	Paleocene–Eocene	Layer VII	–		0.707775	10
VIII/1	Chouabine Fm.	Paleocene–Eocene	Layer VIII	–		0.707759	10
VIII/3	Chouabine Fm.	Paleocene–Eocene	Layer VIII	–		0.707777	11
IX/1	Chouabine Fm.	Paleocene–Eocene	Layer IX	–		0.707815	10
IX/5	Chouabine Fm.	Paleocene–Eocene	Layer IX	–		0.707810	11

[a] Crocodile tooth

(JNdi—Tanaka et al. 2000). The Nd isotope ratios are expressed as

$$\varepsilon_{Nd} = \left[\frac{\left(^{143}Nd/^{144}Nd\right)_{measured}}{\left(^{143}Nd/^{144}Nd\right)^{0}_{CHUR}} - 1 \right] \times 10^{4},$$

where $^{143}Nd/^{144}Nd$ for present-day CHUR is 0.512638 (Jacobsen and Wasserburg 1980).

Results

Strontium isotope ratios: The Early Maastrichtian samples of the El Haria Formation from the Alima Mountain yielded $^{87}Sr/^{86}Sr$ ratios of 0.707795 and 0.707785 for a shark tooth and a coprolite, respectively. In the same sequence, the $^{87}Sr/^{86}Sr$ ratios from Paleocene–Eocene shark teeth of the Chouabine Formation vary between 0.707762 and 0.707821 ($n = 5$), while in coprolites, they range between 0.707769 and 0.707801 ($n = 6$) (Fig. 3).

Sr isotope ratios of Paleocene–Eocene shark teeth from the Chouabine Formation at Kef Eddour vary between 0.707740 and 0.707821 ($n = 17$), while from the Early Eocene Métlaoui *s.s.* Formation, they range from 0.707727 to 0.707741 ($n = 4$). From this later unit, one crocodile tooth was also analyzed, which yielded the highest Sr isotope ratio for the basin with a value of 0.707848.

As a first approximation, all the Sr isotope data are projected on the global ocean Sr evolution curve (McArthur et al. 2001—look-up Table Version 4: 08/04) and are shown in Fig. 3a. The data are presented in stratigraphic order and relative to the Paleocene–Eocene boundary, which is fixed between layers II–IV of the Chouabine Formation based on the reported negative carbon isotope shift (Ounis et al. 2008) and the paleontological work of Ben Abdessalam (1978). Then, where it was possible, the Sr isotope ratios of the fossils were plotted on the global Sr isotope curve layer by layer (cf. Fig. 3a). In certain layers, the $^{87}Sr/^{86}Sr$ ratios show large variation, and considering all the errors, they can range up to 68 ppm. The largest spreads come from layers I, II and VII–VIII of the Chouabine Formation.

In order to compare the Sr isotope data to the McArthur's curve in a more quantitative way, a simple *Z* test was applied:

$$Z_{statistic} = \frac{\bar{X}_{^{87}Sr/^{86}Sr-measured} - \bar{X}_{^{87}Sr/^{86}Sr-curve}}{\sqrt{\left(SE_{^{87}Sr/^{86}Sr-measured}\right)^2 + \left(SE_{^{87}Sr/^{86}Sr-curve}\right)^2}},$$

where $\bar{X}$ and SE stand for the mean and the standard error of the mean, respectively. The mean Sr isotope values for the Sr curve are taken from McArthurs' look-up table between 46 and 70 million years with 1 My steps. The largest 95 % confidence interval of the curve in this period is used to

Table 2 Statistical treatments of $^{87}Sr/^{86}Sr$ ratios of the shark teeth. (a) *Z* test is used to compare each measured $^{87}Sr/^{86}Sr$ ratios to McArthur et al. (2001) global Sr evolution curve with 1 My steps. Values of *Z*-statistic between −1.96 and 1.96 signify that the average $^{87}Sr/^{86}Sr$ ratio for the given layer is not different from the McArthur curve at a probability level of 0.05. In this case, the given age value appears in the table. Those with italics though yielded significant match due to the pattern of the global curve (cf. Fig. 3a), but with respect to the local stratigraphy, they do not have importance. (b) Comparing the variance of the obtained ages for each layer. Note that there is a significant difference between the samples in layer I, II and VII–VIII. (c) These latter layers were further tested by Tukey posteriori statistic, which shows that ZT-2, ZT-6 and VII/-1 are outliers in their corresponding layer (cf. text and Fig. 3b). (d) The calculated average Sr isotope ages for each layer and outlier

Data from McArthur et al. (2001); SE of 0.000011 as a maximum value is used for all the ages.

				Ma	EOCENE											PALEOCENE									CRETACEOUS							(a)	(b) ANOVA	(c) posteriori Tukey statistic	(d) Ma
					46	47	48	49	50	51	52	53	54	55	56	57	58	59	60	61	62	63	64	65	66	67	68	69	70						
					0.707764	0.707751	0.707736	0.707714	0.707714	0.707713	0.707728	0.707729	0.707743	0.707757	0.707771	0.707782	0.707791	0.707798	0.707804	0.707810	0.707814	0.707819	0.707824	0.707828	0.707830	0.707814	0.707796	0.707777	0.707747						
Métlaoui *s.s.* Fm.		PTMt-1	13	0.707740	46	47	48				52	53	54	55															70		$F_{3,10}$ = 1.837	q - Tukey statistic p - probability they have the same mean	47.9 ± 1.3
		PTMt-3	10	0.707727		47	48	49	50	51	52	53	54															70		p= 0.204		
		PTMr-1	11	0.707730		47	48	49	50	51	52	53	54															70				
		PTMr-2	10	0.707741	46	47	48				52	53	54	55															70				
Chouabine Formation	0	0/1	11	0.707740	46	47	48				52	53	54	55															70	$F_{1,7}$ = 0.259		*53.8 ± 1.4*
		0/4	11	0.707749	46	47	48				52	53	54	55	56														70	p= 0.626		
	I	I/3	11	0.707761	46	47							54	55	56	57												69	70	$F_{2,14}$ = 12.810		*55.5 ± 1.2*
		I/4	11	0.707763	46	47							54	55	56	57												69	70	p= 0.001		
		ZT2	11	0.707804												57	58	59	60	61	62	63	64	65	67	68						*61.0 ± 2.7*
	II	II/1	10	0.707750	46	47	48				52	53	54	55	56														70	$F_{2,13}$ = 7.963		*54.0 ± 1.5*
		II/2	11	0.707749	46	47	48				52	53	54	55	56														70	p= 0.006		
		ZT6	17	0.707782	46									55	56	57	58	59	60							68	69					*57.5 ± 1.9*
	III-IV	III-IV/1	11	0.707767	46	47							54	55	56	57	58											69	70	$F_{2,11}$ = 2.357		*55.1 ± 1.7*
		III-IV/2	11	0.707749	46	47	48				52	53	54	55	56														70	p= 0.141		
		ZT8	10	0.707762	46	47							54	55	56	57												69	70			
	V-VI	V/2	11	0.707781	46									55	56	57	58	59	60							68	69			$F_{1,9}$ = 0.223		*57.3 ± 1.7*
		V/3	10	0.707774	46	47								55	56	57	58	59								68	69			p= 0.648		
	VII-VIII	VII/1	14	0.707743	46	47	48				52	53	54	55															70	$F_{4,19}$ = 6.646		
		VII/2	10	0.707775	46	47								55	56	57	58	59								68	69			p= 0.002		*57.2 ± 1.8*
		VIII/1	10	0.707759	46	47	48						54	55	56	57												69	70	⬇		
		VIII/3	11	0.707777	46									55	56	57	58	59								68	69			$F_{2,35}$ = 6.646		*53.5 ± 1.3*
		ZT11	11	0.707786	46										56	57	58	59	60	61						68	69			p= 0.001		
	IX	IX/1	10	0.707815														59	60	61	62	63	64	65	66	67	68			$F_{2,19}$ = 0.123		
		IX/5	11	0.707810													58	59	60	61	62	63	64	65	66	67	68			p= 0.885		61.8 ± 2.2
		ZT12	11	0.707821														59	60	61	62	63	64	65	66	67	68					
El Haria Fm.		K4	11	0.707795											56	57	58	59	60	61	62	63				67	68	69					68.0 ± 1.0

q/p	I/3	I/4	ZT2
I/3	-	1.00	0.00
I/4	0.00	-	0.00
ZT2	5.45	5.45	-

q/p	II/1	II/2	ZT6
II/1	-	1.00	0.01
II/2	0.00	-	0.01
ZT6	4.74	4.74	-

q/p	a VII/1	b VII/2	c VIII/1	d VIII/3	e ZT11
VII/1	-	0.02	0.33	0.02	0.00
VII/2	4.79	-	0.60	1.00	0.60
VIII/1	2.74	2.05	-	0.60	0.06
VIII/3	4.79	0.00	2.05	-	0.60
ZT11	6.85	2.05	4.11	2.05	-

q/p	ac	bcd	bde
ac	-	0.01	0.00
bcd	4.27	-	0.33
bde	6.32	2.04	-

calculate the *Z*-statistic at each time slice. This value is about 22 ppm; hence, a SE of 11 ppm is applied. All of these curve-derived values were compared with each $^{87}Sr/^{86}Sr$ measurement of shark teeth (Table 2). When the *Z* test yields a value between −1.96 and 1.96, the measured $^{87}Sr/^{86}Sr$ fits the curve at that age with 95 % confidence limit. With this calculation, an age matrix can be obtained with all possible Sr ages (Table 2). From Fig. 3a, it is clear that one $^{87}Sr/^{86}Sr$ ratio can match with various ages as the global Sr curve fluctuates, but considering information about the local stratigraphy, some of these ages can be ignored (cf. Table 2).

In the next step, single-factor analyses of the variance (ANOVA) of the meaningful ages were tested within each layer. Where no significant differences appeared among the samples (at $\alpha = 0.05$), the Sr ages were averaged for the given layer. The ANOVA analysis, however, yielded significant differences in the variance for layer I, II and VII–VIII. From a posteriori Tukey statistic, it is evident that ZT-2 from layer I and ZT-6 from layer II are outliers. In the case of layer VII–VIII, the VII/1 is different from all the samples but VIII/3. A further *Student's t test* also proved that the latter is significantly different from ZT-11. This apparent overlapping was further tested by pooling the samples in the three possible groupings, and an ANOVA and Tukey statistic were run again (cf. Table 2). The analyses show that VIII/3 is significantly closer to the rest of the samples than to VII/1; thus, the latter is considered as an outlier. For these three layers, two–two mean ages were calculated: one from the outliers and one from the remaining samples (Table 2).

Neodymium isotope ratios: Few samples from the Alima section were analyzed for Nd isotope ratios, expressed also as ε_{Nd} values (Table 1). While pure coprolite of the Early Maastrichtian phosphate bed and the layer IX of the Chouabine Formation yielded ε_{Nd} values of −9 and −10.2, respectively, the mixed teeth and coprolites have a range from −8.3 to −9.

Oxygen isotope compositions: Shark teeth from the layer 0 of the Chouabine Formation yielded $\delta^{18}O$ values of 19.3 ± 0.5 ‰ ($n = 4$), while in the Métlaoui *s.s.* Formation, $\delta^{18}O$ values of 20 ± 0.5 ‰ ($n = 5$—shark teeth) and 20.5 ‰ ($n = 1$—crocodile tooth) were obtained (Table 2; Fig. 4).

Discussion

Strontium isotope ratios

Preservation of the fossils

Using the strontium isotope ratios of marine fossils for Sr isotope stratigraphy and paleoceanographic investigations, it is assumed that the isotopic ratio remain intact over time.

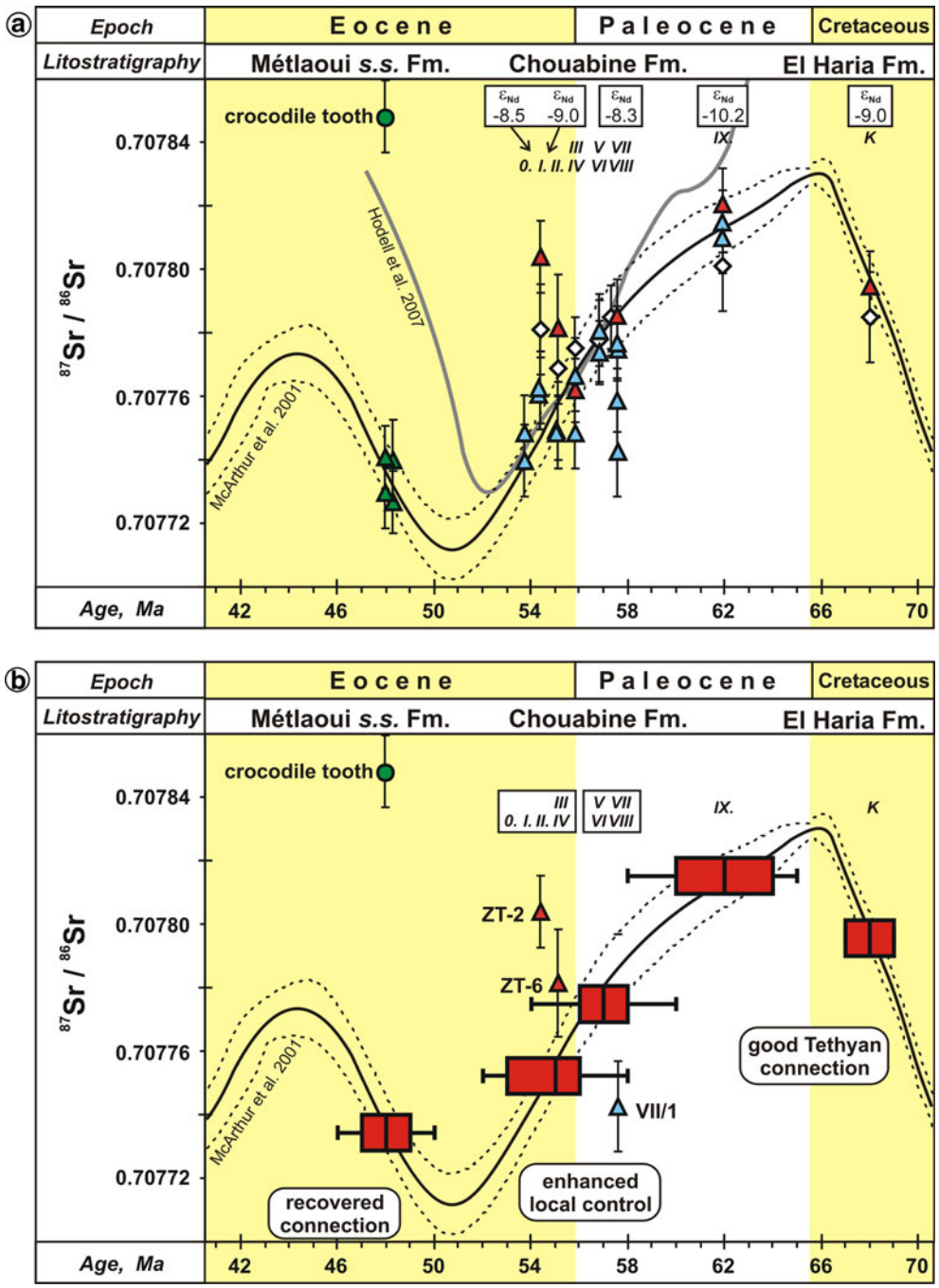

Fig. 3 **a** Strontium isotope ratios of the samples plotted against the global ocean Sr isotope evolution curve (McArthur et al. 2001). The *curve* is shown with *black line* where the *parallel dashed lines* correspond to the 95 % confidence limit on the ages. With *grey line* the data of Hodell et al. (2007) is plotted for comparison (cf. text). Alima Mountain: *red triangles*—shark teeth; *white diamonds*—coprolites. At the layers from where neodymium isotope ratios were analyzed, the ε_{Nd} values are shown accordingly. Kef Eddour: *blue triangles*—shark teeth. Métlaoui *s.s.* Formation: shark teeth—*green triangles*; *green circle*—crocodile tooth. **b** Strontium isotope stratigraphy of the Gafsa Basin with the proposed age ranges displayed by box plots for the given lithostratigraphic units following age-model-1 (cf. text and Table 3). Note that the teeth of ZT-2, ZT-6 and VII/1 are significantly different from the rest of the teeth in their layers (Table 2), and they are not included in the age calculations

However, $^{87}Sr/^{86}Sr$ ratios in phosphatic fossils can be to some extent altered and are not reliable for very precise dating of their enclosing sediments (Schmitz et al. 1997; Barrat et al. 2000), and error in the Sr ages can vary from 0 to 4.5 My (Martin and Scher 2004). Still, many studies demonstrated that when only the well-crystallized and more resistant tooth enameloid is sampled, a relatively good approximation for the depositional time can be

obtained (Ingram 1995; Vennemann and Hegner 1998; Martin and Scher 2004; Kocsis et al. 2007, 2009; Becker et al. 2008).

Bioapatite, like bone and dentin, originally has larger organic content compared to well-crystallized, dense enameloid. During early fossilization, the organic matter degrades and perishes. This process opens more pore space, which allows precipitation of more secondary apatite in bones than in teeth (up to 25 % cf. Trueman and Tuross 2002). At this point, the newly precipitated apatite incorporates Sr from the pore water, and hence, the overall original marine Sr isotope ratios could be partially modified. Similarly, for the coprolites, as they were entirely mineralized in the sediment or at the sediment/water interface, their Sr isotope ratio links rather to the early diagenetic pore fluid. Therefore, if strong diagenetic alteration had occurred, then that would have influenced more the coprolites than tooth enameloid.

In Fig. 3a, offset between the two archives is apparent mainly for the older beds. However, in the younger ones, the deviation is not consistent and the Sr isotope ratios of the coprolites generally overlap with the $^{87}Sr/^{86}Sr$ range of the teeth. This similarity in the Sr isotope ratios and the fact that the Paleogene teeth and coprolites yielded very similar seawater-type rare earth element patterns (Ounis et al. 2008) indicate that the pore fluid chemistry was largely dominated by seawater in the Gafsa Basin.

Interestingly, the crocodile tooth analyzed from the Métlaoui *s.s.* Formation yielded the highest $^{87}Sr/^{86}Sr$ ratios from the Gafsa Basin. This relates to different ecology, most possibly to terrestrial and freshwater habitat in contrast to the shark teeth, which form in the marine realm. The preservation of different environmental Sr isotope ratios in these teeth gives further support that no strong diagenetic alteration took place in these beds. Otherwise, much more homogenized Sr ratios would be expected. Similarly, much higher $^{87}Sr/^{86}Sr$ ratio would be expected for the shark teeth too if some late diagenetic overprint took place in these beds, for example in presence of younger seawater (e.g., Oligocene). Another possibility is that this crocodile tooth was formed in a marine environment and may have been re-deposited from old sediments. The closest such high $^{87}Sr/^{86}Sr$ ratios are at the K/T boundary, though the mean Sr isotope trend from McArthur's curve is below the value of the crocodile tooth (Fig. 3). Below the K/T boundary, the youngest sediments with similar elevated $^{87}Sr/^{86}Sr$ ratios occur in the Triassic, prior to the evolution of this type of crocodile. Furthermore, the good preservation of the tooth does not support any of these long-term re-working; hence, the marine origin of this crocodile tooth is rejected here.

Altogether, if partial modification of the original Sr isotope ratios in the shark teeth occurred, that was very minor relative to coprolites and to the variation observed in certain beds. This is supported by (1) the good preservation of the fossils (Ounis et al. 2008), (2) the preserved different habitat conditions in the Sr isotope ratios between continental and marine organisms, and (3) the similar Sr isotope ratios between pore fluid and seawater indicated by the coprolites.

Strontium isotope stratigraphy

The overall range in the Sr isotope measurements of the phosphatic remains is evidently in the expected open ocean variation, whenever the data are compared to the global Sr isotope curve of McArthur et al. (2001) (Fig. 3a) or to the compilation of Veizer–Prokoph (Veizer et al. 1999; Prokoph et al. 2008). Moreover, the data generally agree with the expected time range of these phosphate beds (Chaabani and Ben Abdelkader 1992; Bolle et al. 1999). In order to obtain more quantitative Sr isotope ages, from now the data are only compared to McAthur's Sr database because it provides straightforward absolute ages with 95 % confidence limit for a certain $^{87}Sr/^{86}Sr$ ratio and it is based on Sr isotope ratios from well-preserved samples and from well-dated localities (McArthur and Howarth 2004). However, an important issue about McArthur's Sr isotope curve is its resolution. There are periods where the curve is defined only by few data points, which bears larger uncertainties. One of the critical periods is in fact the Paleocene, which has importance in this study; therefore, it is further discussed.

Recently, Hodell et al. (2007) carried out a detailed Sr isotope study on foraminifers from the Walvis Ridge to improve the curve with new Paleocene–Eocene data. These fossils were scrutinized by secondary electron microscopy showing good preservation, but the analyses also revealed secondary calcite precipitations in the tests. The pore fluids have very high Sr isotope ratios in these sediments; consequently, the presence of some diagenetic Sr with high $^{87}Sr/^{86}Sr$ in the bulk foraminifera analyses is inevitable. Therefore, the authors provided a weighted curve fit through the lowest $^{87}Sr/^{86}Sr$ values (Fig. 3a). This line is undistinguishable from McArthur's curve between 52 and 58 Ma (Fig. 3a) and hence supports the integrity of the curve over this interval. Conversely, some of Hodell et al.'s data deviate toward higher $^{87}Sr/^{86}Sr$ ratios, particularly in the Early Eocene (cf. Fig. 3a), which could be due to higher proportion of the mentioned secondary calcite precipitate. Moreover, with respect to our data from the Early Eocene phosphate beds, shark teeth can be easily placed on the McArthur's curve, while the terrestrial crocodile tooth is rather in the range of Hodell's data. Though further fine-tuning of the global Sr isotope curve is needed, the data from the Gafsa Basin are converted to absolute ages with

the aid of McArthur's most updated database (Tables 2, 3; Fig. 3b).

After statistical comparison between the shark teeth data and the global curve, and then the elimination of the outliers, meaningful Sr isotope ages can be assigned for the studied layers (Tables 2, 3). The $^{87}Sr/^{86}Sr$ ratio of the shark tooth from the El Haria Formation gives a Sr isotope age of 68 ± 1 Ma (Fig. 3), which agrees with the reported Early Maastrichtian age of these beds (e.g., Chaabani and Ben Abdelkader 1992; Keller et al. 1998).

The Chouabine Formation shows much larger variations in Sr isotope ratios, though the overall Sr age range (Fig. 3b) is in accordance with the general time period proposed for these phosphorites (Ben Abdessalam 1978; Chaabani and Ben Abdelkader 1992; Bolle et al. 1999; Ounis et al. 2008; Zili 2010). To the oldest phosphate bed, layer IX, a Sr age of 61.8 ± 2.2 Ma can be assigned. The large error mainly relates to the shape of the global curve at this time, rather than to the scatter of the data (Fig. 3). The age range corresponds to middle–late Paleocene. The upper array, however, may not reflect the real depositional age of these sediments (Chaabani 1995) because this layer consists of many re-worked elements. Hence, the analyzed teeth could also derive from older sediments, and their Sr isotope ratios may reflect episodes of marine sedimentation from which no sediment was preserved in the basin.

For the rest of the Chouabine Formation, several age-models can be considered (Table 3), if the evident outliers are taken out. Layers V–VI and VII–VIII would result in almost identical Sr ages ($t_{(29)} = -0.18$; $p < 0.05$) with an average of 57.2 ± 1.8 Ma. For the younger beds, pair-wise comparisons from older to younger layers would not show significant differences among them, except layer I, which shows slightly older Sr age compared to the layers underneath and above. However, pooling all the ages together would not make any significant differences with or without the data from layer I, and an age of 54.6 ± 1.6 Ma can be proposed for the upper part of the Chouabine Formation (Fig. 3b; Table 3).

However, exclusive of layer I, the phosphate beds show a decreasing age trend, and given the fact that a negative $\delta^{13}C$ shift was detected at layer III–IV (Fig. 2, Ounis et al. 2008), plus layer 0 yielded notably different $\delta^{18}O$ values (Fig. 5) relative to the other layers, an alternative, more subtle age-model can be considered with the following ages: 55.1 ± 1.7 Ma (III–IV), 54 ± 1.5 Ma (II) and 53.8 ± 1.4 Ma (0) (cf. age-model-2, Table 3). But again, with respect to the mean $^{87}Sr/^{86}Sr$ ratios, these layers (0, II and III–IV) are not significantly different.

The youngest shark teeth from the phosphorite beds of the Métlaoui *s.s.* Formation (Fig. 2a) yielded the lowest Sr isotope ratios in the Gafsa Basin (Fig. 3). These $^{87}Sr/^{86}Sr$ could match with three different Sr isotope ages on the global curve in the Eocene (Fig. 3). However, the 47.9 ±

Table 3 Different age-models derived from comparison of the $^{87}Sr/^{86}Sr$ ratio of the shark teeth with McArthur et al. (2001) global Sr evolution curve. Note that the most likely and statistically most significant is the Age-model-1 (cf. text and Fig. 3b)

Métlaoui s.s. Fm.		PTMt-1 PTMt-3 PTMr-1 PTMr-2	**47.9 ± 1.3**			
Chouabine Formation	**0**	0/1 0/4	*53.8 ± 1.4*	***Age model - 1***	***Age model - 2*** **53.8 ± 1.4**	***Age model - 3***
	I	I/3 I/4 ZT2	*55.5 ± 1.2* *61.0 ± 2.7*	*re-deposited (1)*	re-deposited (3)	*re-deposited (1)*
	II	II/1 II/2 ZT6	*54.0 ± 1.5* *57.5 ± 1.9*	**54.6 ± 1.6** *re-deposited (1)*	**54.0 ± 1.5**	*re-deposited (1)*
	III-IV	III-IV/1 III-IV/2 ZT8	*55.1 ± 1.7*		**55.1 ± 1.7**	**54.6 ± 1.6**
	V-VI	V/2 V/3	*57.3 ± 1.7*			*re-deposited (2)*
	VII-VIII	VII/1 VII/2 VIII/1 VIII/3 ZT11	*57.2 ± 1.8* *53.5 ± 1.3*	**57.2 ± 1.8** *?? Local control (1)*	**57.2 ± 1.8** *?? Local control (1)*	*re-deposited (3)*
	IX	IX/1 IX/5 ZT12	**61.8 ± 2.2**			
El Haria Fm.		K4	**68.0 ± 1.0**			

1.3 Ma, corresponds to early Lutetian, is the most reasonable concerning local stratigraphy, as well as the proposed age range for the Métlaoui *s.s.* Formation (e.g., Chaabani 1995; Zaïer et al. 1998).

Strontium isotope ratio as paleoenvironmental proxy

The evident outlier samples in some layers call for further explanations. ZT-2 and ZT-6 are above the global Sr isotope curve, while VII/1 is below (Fig. 3b), which could mean that different local processes took place in the basin.

The global Sr isotope curve decreases during the Paleocene–Eocene (McArthur et al. 2001); hence, the samples with high $^{87}Sr/^{86}Sr$ ratios could have been re-deposited from exposed, older Paleocene phosphate beds (Fig. 3b). Sedimentological evidence for such a process is better known for layer IX in the Chouabine Formation (Chaabani 1995), because this layer consists of many re-worked elements, and also the shark teeth have slightly more worn appearance. Curiously, teeth from this layer both from Alima and Kef Eddour yielded consistent $^{87}Sr/^{86}Sr$ ratios relative to the more scattered data in the younger beds of the Chouabine Formation.

Long-term sea-level trend falls during the Paleocene and the earliest Eocene (Miller et al. 2005), which could have a major effect on the shallow intracratonic Gafsa Basin. This could result in exposure of the older sediments that could easily erode back into the basin. How extensive this process was is hard to assess, but the outsider teeth of ZT-2 and ZT-6 are best to explain by re-deposition from Paleogene beds. However, comparing the remaining samples from layer I to the beds above and below, here the relative higher Sr isotope ratios can also be indicative for re-working.

Moreover, if the whole basin was affected much earlier by sea-level drop, an alternative third age-model may be proposed with assuming that the lowest $^{87}Sr/^{86}Sr$ ratio of VII/1 in the layers VII–VIII (Fig. 3b) represents the actual global seawater value. Then, the remaining teeth from layers V–VI and VII–VIII should be considered as re-worked specimens, and an overall absolute age of 54.6 ± 1.6 Ma can be calculated for the upper units of the Chouabine Formation (cf. age-model-3 in Table 3). This would imply that there are five to six teeth that are outliers relative to one. Hence, other explanation for the low $^{87}Sr/^{86}Sr$ of VII/1 tooth would be more realistic.

The most straightforward process would be early diagenesis in the presence of younger seawater or contact with pore waters affected by older Mesozoic carbonates, both of which could shift the $^{87}Sr/^{86}Sr$ toward lower values (e.g., Elderfield and Gieskes 1982, Martin and Scher 2004). These types of alteration can be clearly seen on the Sr isotope ratios of the coprolites from layer IX and the Cretaceous bed, though the offsets from the teeth are not too large here. However, in the layers V–VI and VII–VIII, the coprolites show high $^{87}Sr/^{86}Sr$ similar to the majority of the teeth (Fig. 3a). This similarity weakens the hypothesis that the low Sr ratios in the well-preserved shark tooth enameloid are due to early diagenetic modification.

Another explanation for the low $^{87}Sr/^{86}Sr$ values could be locally controlled seawater (e.g., Flecker and Ellam 2006; Topper et al. 2011). This means extra, surplus Sr input with different isotope ratios into the Gafsa Basin or some of its more restricted parts, where the seawater could not have completely mixed with the open sea. Hence, the Sr isotope ratio of the local seawater was different from the global ocean value. If sharks swam and stayed occasionally in this modified seawater, their teeth could have recorded and retained this isotopic ratio. However, the general problem with the modified seawater scenario is that seawater contains hundred times more Sr than an average river would bring into the ocean (e.g., Palmer and Edmond 1992). Then, the amount of Sr needed to change the seawater $^{87}Sr/^{86}Sr$ would result in brackish or freshwater milieu.

Nevertheless, Late Cretaceous marine carbonates are abundant in the wider region of the Gafsa Basin (e.g., Abdallah et al. 1995, 2000; Mabrouk et al. 2006; Lazzez et al. 2008), and these sediments are known to have low Sr isotope ratios (McArthur et al. 2001). Clear paleontological evidence for active re-working of such rocks is documented by the presence of large amount of upper Cretaceous, calcareous nannofossils that occur in many intercalated marl beds of the Chouabine Formation (e.g., Bolle et al. 1999). Therefore, some Cretaceous strata were apparently uplifted by the end of the Cretaceous (Bolle et al. 1999; Bouaziz et al. 2002) and could be a potential low Sr isotope source for river input. Moreover, in the early Paleogene, a warm greenhouse climate existed with elevated CO_2 concentration in the atmosphere (Pearson and Palmer 2000; Zachos et al. 2001), and when such conditions couple with high humidity, that could enhance chemical weathering of carbonates. Such humid, warm conditions were recognized in Tunisia at this time inferred from investigation on bulk rock and clay mineralogy (Adatte et al. 2002). Given these combined circumstances, it is plausible that Paleogene rivers had high dissolved Sr content.

The most prospective beds that could influence river compositions at the time are the limestone of the Abiod Formation (Campanian–earliest Maastrichtian, ~83.5–69.5 Ma) and essentially the marl of the Aleg Formation (uppermost Turonian–Santonian, ~90–83.5 Ma). But also a 200–300-m-thick Late Cretaceous marine carbonate series can be found in the actual Dahar plateau (Djeffara Island) with mid-late Cenomanian to early Coniacian ages (~97.5–87 Ma). From McArthur's look-up table, average

Sr isotopic ratios of 0.707621 (83.5–69.5 Ma) and 0.707353 (97.5–83.5 Ma) can be obtained for these periods and used as $^{87}Sr/^{86}Sr$ ratios for river input. Then, with a simple mass balance calculation, the mixing of these rivers with the seawater in the Gafsa Basin can be testified:

$$^{87}Sr/^{86}Sr_{Gafsa} = {}^{87}Sr/^{86}Sr_{sea} \times f_{sea} \times [Sr]_{sea}/[Sr]_{Gafsa} + {}^{87}Sr/^{86}Sr_{river} \times (1 - f_{sea}) \times [Sr]_{river}/[Sr]_{Gafsa}$$

where subscript for $^{87}Sr/^{86}Sr$ ratios and [Sr] concentrations marked as "Gafsa," "sea" and "river" denote the seawater compositions in the Gafsa Basin, in the open sea and the freshwater compositions of the river input, respectively.

The open-sea Sr concentration is fixed at 8 ppm which is the actual global average value (Bruland and Lohan 2003), and for the open-sea isotopic ratio $^{87}Sr/^{86}Sr = 0.707768$ is chosen from the P/E boundary following the look-up table of McArthur et al. (2001). The Sr concentrations of the Gafsa seawater were calculated at each mixture line with three different river water concentrations: a silica end-member with 0.1 ppm, followed by a more conservative carbonate value of 1 ppm, and a rather excessive one of 4 ppm (e.g., Goldstein and Jacobsen 1987; Palmer and Edmond 1989, 1992; Huh et al. 1998).

The modified seawater $^{87}Sr/^{86}Sr$ ratio in the Gafsa Basin is represented by the VII/1 shark tooth (Table 2: 0.707743). On Fig. 4, when the different mixing lines cross this value, on the *x*-axis, f_{sea} returns the fraction of open seawater in this modified Gafsa seawater composition. The figure clearly shows that the lower the $^{87}Sr/^{86}Sr$ ratios are the less Sr is needed in order to get the measured low $^{87}Sr/^{86}Sr$ ratio from this tooth. Yet, reasonable mixtures could be obtained for marine-brackish (e.g., $f_{sea} = 0.68$ $[Sr]_{river} = 1$ ppm, $^{87}Sr/^{86}Sr = 0.707353$), or with higher Sr load, for marine environments (e.g., $f_{sea} = 0.88$ $[Sr]_{river} = 4$ ppm, $^{87}Sr/^{86}Sr = 0.707353$). If such situation existed, it was maybe very local even inside the Gafsa Basin. But according to the mixing calculation, rivers draining Late Cretaceous marine sediments may have as well influenced the local seawater Sr isotopic ratio. Moreover, the related salinity drop could have been partly compensated by enhanced evaporation, which also occurred at this time (cf. chapter on oxygen isotope composition).

The question is raised whether the observed high $^{87}Sr/^{86}Sr$ ratios could similarly be linked to modified seawater. Normally, weathering of old crystalline rock can provide high $^{87}Sr/^{86}Sr$; however, such rocks are unknown in the nearby region of the Gafsa Basin, and moreover, the Sr content of this type of rocks is generally low. Exposed rocks with high $^{87}Sr/^{86}Sr$ ratio are indicated by the crocodile tooth from the Métlaoui *s.s.* Formation; however, this could be very restricted, and maybe it links to local occurrence of Triassic carbonates and evaporites (Jallouli et al. 2005; Zouaghi et al. 2005; Al-Aasm and Abdallah 2006). Hence, the shark teeth with higher $^{87}Sr/^{86}Sr$ ratio than the global ocean are preferred to interpret as re-worked specimens.

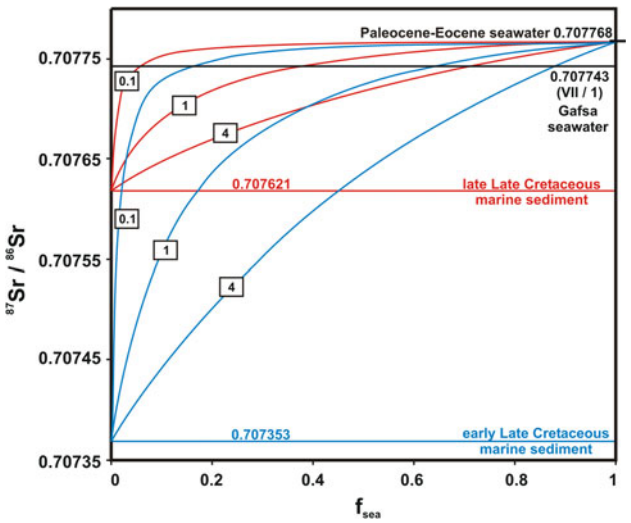

Fig. 4 Mixing scenarios between seawater and theoretical Sr inputs to demonstrate the possible local effects on the seawater $^{87}Sr/^{86}Sr$ ratio in the Gafsa Basin, with low $^{87}Sr/^{86}Sr$ sources. The composition of the Paleocene–Eocene seawater is taken from the stage boundary (55.8 Ma) following the lookup table of McArthur et al. (2001). Similarly, the Late Cretaceous seawater $^{87}Sr/^{86}Sr$ ratios are after McArthur et al. (2001), and these are the averages between 97.5 and 83.5 Ma (*blue lines*) and 83.5–69.5 Ma (*red lines*), respectively. These Sr isotopic ratios represent possible river compositions assuming that these rivers drained on Late Cretaceous marine sediments. The mixing calculations were performed with three different Sr concentrations of 0.1, 1 and 4 ppm. Note that the higher the Sr concentration in the input source and the larger the differences in Sr isotope ratio between the open-sea and the input source, the more realistic marine conditions can be obtained for the mixture

Neodymium isotope ratios

The ε_{Nd} values from the Gafsa Basin are non-radiogenic (Fig. 3a). The results are similar to those reported from the phosphorite deposits of Morocco and Tunisia (Grandjean et al. 1987; Soudry et al. 2006), although from the Paleogene series of Morocco, more radiogenic values were analyzed as well (Grandjean et al. 1987). The ε_{Nd} values are also similar to those of contemporaneous Atlantic deepwater (Thomas et al. 2003), which might suggest links between these basins as having a common water source. However, the Sr isotope results in some cases indicate important local factors in the Gafsa Basin, and moreover because of the short residence time of Nd in seawater, connecting these basins on the basis of a few Nd isotope ratios is very uncertain. In contrary, Stille et al. (1996) and Pucéat et al. (2005) reported ε_{Nd} values for the Late Cretaceous Tethys Ocean, which also cover the ε_{Nd} range from the Gafsa Basin. Water exchanges between the Gafsa Basin and the

Tethys is known at this time (Fig. 1b), hence our Nd data confirm this relation rather than an Atlantic connection.

Although only few Nd isotope ratios were analyzed, their relative similarities to other phosphorite deposits and to Early Paleogene and Late Cretaceous Tethyan seawater support preservation of marine values. The results are therefore consistent with the Sr isotope data used for dating the sediments, but even with the paleoenvironmental interpretations derived from the outlier samples. Such as re-working or possible locally affected seawater composition by Late Cretaceous marine carbonates would not have resulted in exceptionally different Nd isotope ratios.

Oxygen isotope composition

The oxygen isotope analyses of shark teeth from the top phosphate bed (layer 0) of the Chouabine Formation and from the Métlaoui *s.s.* Formation are extensions of the previous isotope dataset analyzed from the Gafsa Basin (Fig. 5; Ounis et al. 2008). These new measurements show the lowest $\delta^{18}O$ values in comparison with the rest of the Paleogene samples. Only one Maastrichtian shark tooth from the El Haria Formation is in the range of these low isotopic values (Fig. 5).

The oxygen isotope composition of shark teeth is a function of the oxygen isotope composition of seawater and water temperature (e.g., $T(°C) = 113.3–4.38 \times (\delta^{18}O_{PO_4} - \delta^{18}O_{H_2O})$ cf. Longinelli and Nuti 1973; Kolodny et al. 1983). Assumptions about seawater isotopic composition can induce uncertainty on temperature calculations. To illustrate this, in Fig. 5, temperature scales are plotted and calculated on the basis of two seawater oxygen isotope compositions. The first with $\delta^{18}O_{H_2O}$ value of −1 ‰ represents Greenhouse open ocean conditions (Lear et al. 2000), such as the Late Cretaceous–Early Paleogene period, while the second with $\delta^{18}O_{H_2O} =$ 0 ‰ assumes more evaporative seawater that can occur at low latitude and in confined basins.

The higher $\delta^{18}O_{PO_4}$ values derived from the layers I–IX of the Chouabine Formation indicate a colder temperature range when they are compared to the top layer 0, assuming a constant $\delta^{18}O_{H_2O}$ for the seawater. However, if a similar overall habitat temperature is assumed for these sharks, then clearly more evaporative seawater is required for the older part of the section to maintain this. From the latter, it would follow that the Gafsa Basin was relatively more restricted at this time, which agrees with the Sr isotope data, at least for the layers I–VIII. Furthermore, all these would support the hypothesis of why the observed large negative $\delta^{13}C$ excursion did not couple with the recognizable hyperthermal shift in the $\delta^{18}O$ values (Ounis et al. 2008) between layer II and IV in the Chouabine Formation.

Fitting a second-order running average trend on the oxygen isotope data reveals a negative shift on the top of the sedimentary sequence. Comparing the $\delta^{18}O$ means of the layers exposes significant differences between the older layers (I–IX) and the younger beds (layer 0 and Métlaoui beds) (e.g., for the pooled dataset applying *Student's t test* assuming unequal variances: $t_{(11)} = 4.16$; $p < 0.05$). Hence, this $\delta^{18}O$ shift could relate to significant environmental changes. From the view of the Sr isotope data, it can be interpreted that the basin started maintaining once more, better connection with the open sea (Figs. 3b, 6), and this change could have been driven by global sea-level rise (Miller et al. 2005).

It must be mentioned that the low $\delta^{18}O$ values observed in these fossils could be linked to enhanced freshwater input as well. However, in the view of the Sr isotope results, since these samples exhibit closer values to the open ocean Sr isotope curve than the teeth from the layer underneath, the preferred interpretation is the re-established better connection with the open ocean (Figs. 3b, 6).

The low $\delta^{18}O$ values of these shark teeth could also indicate warm seawater temperature, and it might coincide with the Early Eocene Climatic Optimum (EECO—Zachos et al. 2001). This event is a result of a long-term warming trend from the Late Cretaceous onwards, which peaked between 51 and 53 Ma (Zachos et al. 2001). Despite the possible local effects on the Sr isotope ratios, the teeth from layer 0 yielded Sr isotope ages that are very close to the peak of the EECO event (cf. age-model-2, Table 3). Nevertheless, local influence is a clear issue in the Gafsa Basin; hence, further studies are necessary to clarify the exact relation of these low $\delta^{18}O$ values to the EECO.

Paleoenvironment

Strontium and oxygen isotope analyses of shark teeth revealed two different marine conditions in the Gafsa Basin (Fig. 6). In the periods when the teeth yielded consistent $^{87}Sr/^{86}Sr$ and $\delta^{18}O$ compositions similar to global values, the basin maintained good connection with the open ocean. Regarding the phosphate beds, such situation could exist during the deposition of the Early Maastrichtian El Haria Formation and the Early Eocene Métlaoui *s.s.* Formation, but most possibly in the cases of layer 0 and layer IX of the Chouabine Formation too.

Conversely, during the deposition of the major phosphate beds of the Chouabine Formation, the basin had occasional limited connection with the open sea in the east, which was driven by sea-level drop. This is exhibited by the large variation in the $^{87}Sr/^{86}Sr$ ratios of the shark teeth. Deviation from the open ocean Sr evolution curve to lower Sr isotope ratios is probably due to the weathering of Late Cretaceous carbonates from the hinterland into the basin, which is also supported by micropaleontological data (Bolle et al. 1999). The high $^{87}Sr/^{86}Sr$ ratios in the shark teeth could be explained by re-deposition of the teeth from older

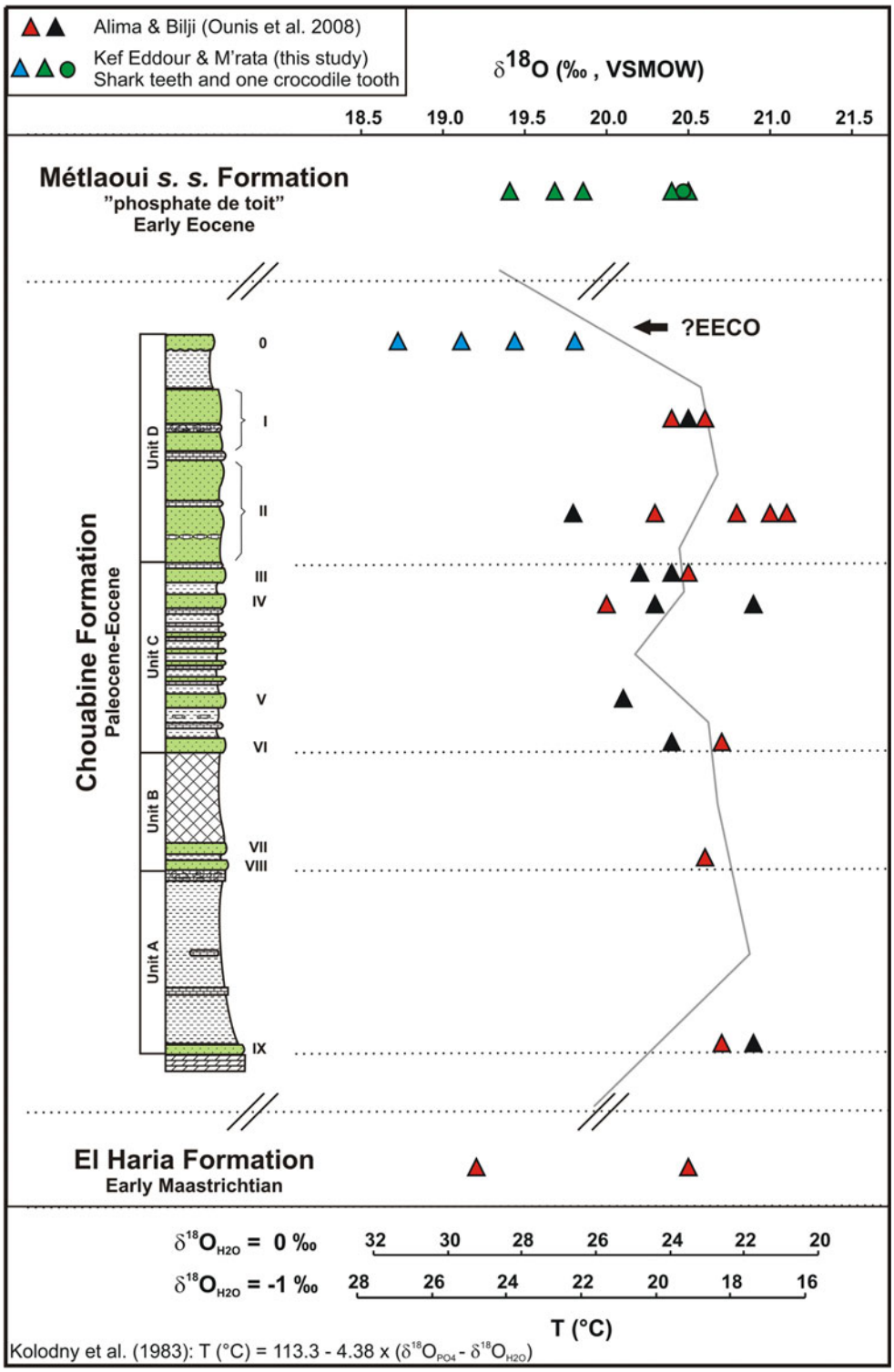

Fig. 5 Oxygen isotope compositions of shark teeth (*green* and *blue triangles*) and crocodile tooth (*green circle*) from layer 0 of the Chouabine Formation and from the Métlaoui *s.s.* Formation. *White* and *red triangles* are $\delta^{18}O$ values of shark teeth from Bliji and Alima Mountains, respectively, after Ounis et al. (2008). The *gray line* across the data is the second-order running average trend on the mean $\delta^{18}O$ values of shark teeth in each layer. The shift to more negative values on the top may link to the Early Eocene Climatic Optimum (EECO). At the *bottom*, seawater temperatures are calculated using the equation of Kolodny et al. (1983) with seawater oxygen isotopic composition of −1 and 0 ‰, representing open Greenhouse and partially restricted evaporative conditions, respectively

beds. The oxygen isotope data from these teeth support the partial restriction of the basin, and the relatively higher $\delta^{18}O$ values could be linked to enhanced evaporation.

Such environmental settings had been recognized and described in the Gafsa Basin earlier (Sassi 1974; Chaabani 1995; Zaïer et al. 1998, Bolle et al. 1999). In this work, the strontium, neodymium and oxygen isotope data of the fossils further confirm these studies with providing new independent evidences and novel insight into the evolution of the Paleogene Gafsa Basin.

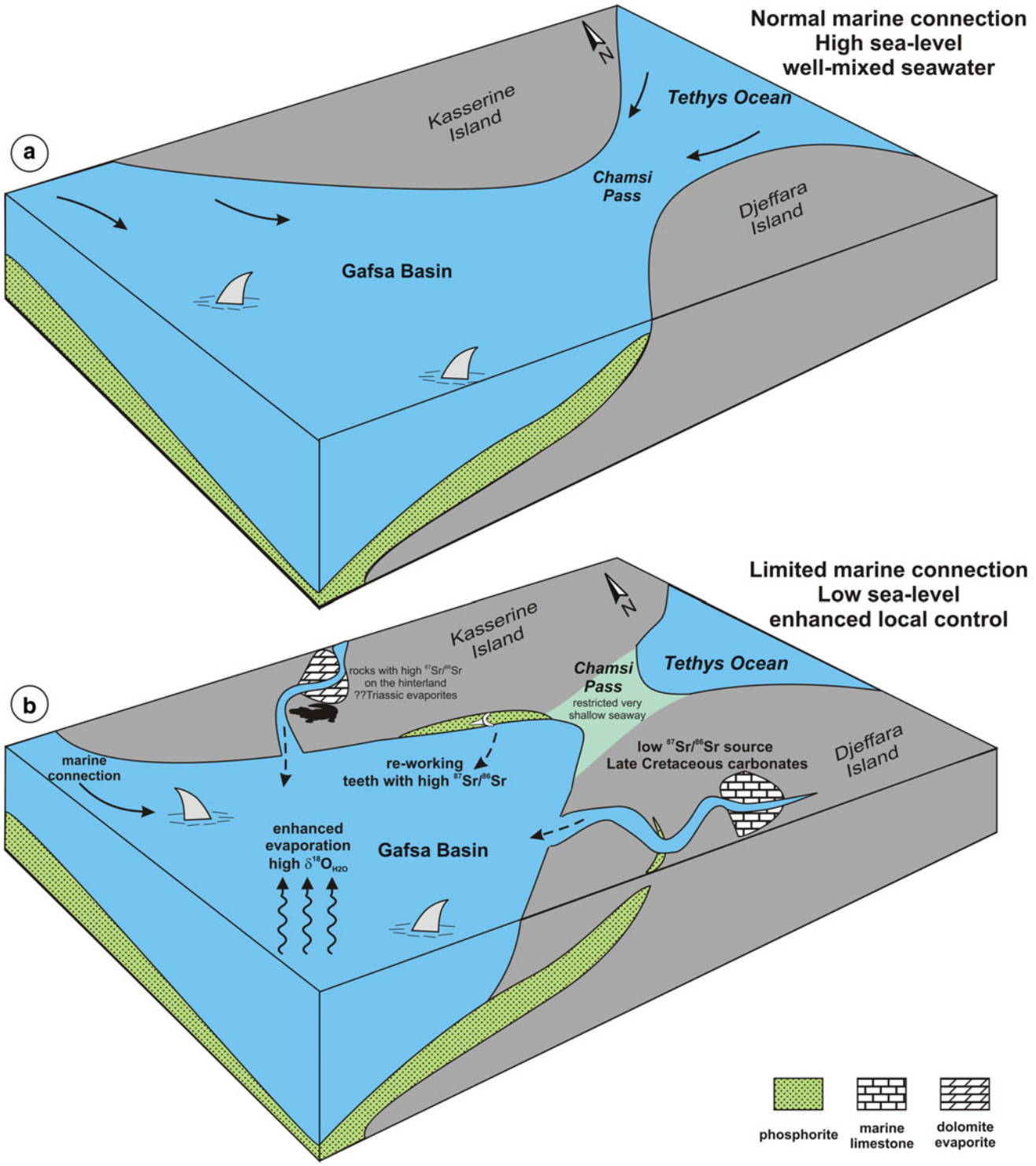

Fig. 6 Paleoenvironmental conditions in the Gafsa Basin based on the geochemical composition of the phosphatic fossils. **a** Normal connection is maintained with the open sea. **b** Increased restriction in the Gafsa Basin. Re-working of older phosphate beds and weathering of Late Cretaceous carbonates were the main processes that are responsible for the observed variation in $^{87}Sr/^{86}Sr$ ratio of the shark teeth

Conclusion

Strontium isotope analyses of the phosphatic fossils from the Gafsa Basin returned meaningful absolute ages for the different Late Cretaceous–Early Paleogene phosphate beds; hence, knowledge about the local stratigraphy has been widened and improved. The following Sr isotope ages are proposed for the different Formations:

- El Haria Formation, Early Maastrichtian: 68 ± 1 Ma
- Chouabine Formation, Paleocene–Eocene: layer IX: 61.8 ± 2.2 Ma; layers VIII–V: 57.2 ± 1.8; layers IV–0: 54.6 ± 1.6 Ma
- Métlaoui *s.s.* Formation, Early Eocene: 47.9 ± 1.3 Ma

Outlier samples from the Chouabine Formation are indicative of local influences and special depositional conditions. The fossils with high $^{87}Sr/^{86}Sr$ ratios are most possibly re-worked from older sediments, while the low $^{87}Sr/^{86}Sr$ in one tooth could be a result of diagenesis. However, the latter may rather reflect the influence of Late Cretaceous marine sediments on the local seawater in the Gafsa Basin, which is supported by model calculation as well. All these are compatible with a dynamic shallow-water milieu in the Gafsa Basin under the influence of sea-level fluctuation.

The ε_{Nd} values of the fossils are similar to those reported from other phosphorite deposits from North Africa and also to those of Late Cretaceous Tethyan seawater.

Oxygen isotope data from shark teeth of the youngest bed of the Chouabine Formation (layer 0) and of the Métlaoui *s.s.* Formation reflect better connection with the open ocean, and the low $\delta^{18}O$ values could be possibly linked to the warm global EECO event.

Acknowledgments The authors are grateful for all the support and help they received from the *Compagnie des Phosphates de Gafsa, Tunisia* for conducting this research with productive fieldwork. We thank M. Cooper for his assistance with TIMS analyses. L. K. was generously funded by the Swiss National Science Foundation (SNF PBLA2-119669 and SNF PZ00P2_126407) and NERC (NE/C00390X/1) projects. Constructive comments by Dr. J. A. Chamberlain and two anonymous reviewers are very much appreciated.

References

Abdallah H, Memmi L, Damotte R, Rat P, Magniez-Jannin F (1995) Le Crétacé de la chaîne nord des Chotts (Tunisie du centre sud): biostratigraphie et comparaison avec les régions voisines. Cretac Res 16:487–538

Abdallah H, Sassi S, Meister C, Souissi R (2000) Stratigraphie séquentielle et paléogéographie à la limite Cénomanien-Turonien dans la région de Gafsa-Chotts (Tunisie centrale). Cretac Res 21:35–106

Adatte T, Keller G, Stinnesbeck W (2002) Late Cretaceous to early Paleocene climate and sea-level fluctuations: the Tunisian record. Palaeogeogr Palaeoclimatol Palaeoecol 178:165–196

Al-Aasm IS, Abdallah H (2006) The origin of dolomite associated with salt diapirs in central Tunisia: preliminary investigations of field relationships and geochemistry. J Geochem Explor 89:5–9

Arsouze T, Dutay J-C, Lacan F, Jeandel C (2009) Reconstructing the Nd oceanic cycle using a coupled dynamical—biogeochemical model. Biogeosciences 6:2829–2846

Aubry MP, Berggren WA, Stott L, Sinha A (1996) The upper-Paleocene-lower Eocene stratigraphic record and the Paleocene-Eocene boundary carbon isotope excursion: implications for geochronology. In: Knox RWO'B, Corfield RM, Dunay RE (eds) Correlation of the early Paleogene in Northwest Europe, vol 101. Geol Soc London Spec Publ, pp 353–380

Bains S, Corfield RM, Norris G (1999) Mechanisms of climate warming at the end of the Paleocene. Science 285:724–727

Barrat JA, Taylor RN, André JP, Nesbitt RW, Lécuyer C (2000) Strontium isotopes in biogenic phosphates from a neogen marine formation: implications for palaeoseawater studies. Chem Geol 168:325–332

Becker MA, Seidemann DE, Chamberlain JA Jr, Buhl D, Slattery W (2008) Strontium isotopic signatures in the enameloid and dentine of upper Cretaceous shark teeth from western Alabama. Paleoecologic and geochronologic implications. Palaeogeogr Palaeoclimatol Palaeoecol 264:188–194

Béji-Sassi A (1999) Les phosphates dans les bassins paléogènes de la partie méridionale de l'Axe Nord-Sud (Tunisie). Thèse Doct. Etat, Univ. Tunis II, Tunisie

Belayouni H (1983) Etude des la matière organique dans la série phosphatée du bassin de Gafsa-Métlaoui (Tunisie): application à la compréhension des mécanismes de la phosphatogenèse. Thèse Doct. ès-Sci. Univ. Orléans, France

Ben Abdessalam N (1978) Etude palynologique et micro-paléontologique de la série phosphatée du bassin de Gafsa-Métlaoui (Tunisie). Application à la compréhension des mécanismes de la phosphatogenèse. Thèse 3ème cycle, Univ. Paris VI, France

Ben Hassen A, Trichet J, Disnar J-R, Belayouni H (2009) Données nouvelles sur le contenu organique des dépôts phosphatés du gisement de Ras-Draâ (Tunisie). C R Geosci 341:319–326

Ben Hassen A, Trichet J, Disnar J-R, Belayouni H (2010) Pétrographie et géochimie comparées des pellets phosphatés et de leur gangue dans le gisement phosphaté de Ras-Draâ (Tunisie). Implications sur la genèse des pellets phosphatés. Swiss J Geosci 103:457–473

Bolle PM, Adatte T, Keller G, Von Salis K, Burns S (1999) The Paleocene-Eocene transition in the southern Tethys (Tunisia): climatic and environmental fluctuations. Bull Soc Géol Fr 170:661–680

Bouaziz S, Barrier E, Soussi M, Turki MM, Zouari H (2002) Tectonic evolution of the northern African margin in Tunisia from paleostress data and sedimentary record. Tectonophysics 357: 227–253

Bruland KW, Lohan MC (2003) Controls of trace metals in Seawater. In: Holland HD, Turekian KK (eds) Treatise on geochemistry, vol 6. Elsevier Ltd, CA, USA, pp 23–47

Burke WH, Denison RE, Hetherington EA, Koepnick RB, Nelson HF, Otto JB (1982) Variation of seawater $^{87}Sr/^{86}Sr$ throughout Phanerozoic time. Geology 10:516–519

Burollet PF (1956) Contribution à l'étude stratigraphique de la Tunisie Centrale, vol 18. Annales des Mines et de la Géologie, Tunis, p 352

Burollet PF, Oudin JL (1980) Paléocène et Eocène en Tunisie, pétroles et phosphates. Géologie comparée des gisements de phosphates et de pétroles. BRGM 24:205–216

Cayeux L (1941) Les phosphates de chaux sédimentaires de France (France métropolitaine et d'outre-mer). Imprimerie nationale, Paris

Chaabani F (1995) Dynamique de la partie orientale du bassin de Gafsa au Crétacé et au Paléogène: Etude minéralogique et géochimique de la série phosphatée Eocène, Tunisie méridionale. Thèse Doc. Etat. Univ. Tunis II. Tunisie

Chaabani F, Ben Abdelkader O (1992) Nouvelles données stratigraphiques sur le Paléocène du Bassin de Gafsa: Conséquence paléogéographique. Note Serv Géol De Tunisie 59:77–87

Dansgaard W (1964) Stable isotopes in precipitation. Tellus 16:436–468

Dettman DL, Kohn MJ, Quade J, Ryerson FJ, Ojha TP, Hamidullah S (2001) Seasonal stable isotope evidence for a strong Asian monsoon throughout the past 10.7 m.y. Geology 29:31–34

Elderfield H, Gieskes JM (1982) Sr isotopes in interstitial waters of marine sediments from Deep Sea Drilling Project cores. Nature 300:493–497

Elderfield H, Pagett R (1986) Rare earth elements in ichthyoliths: variations with redox conditions and depositional environment. Sci Total Environ 49:175–197

Flecker R, Ellam R (2006) Identifying Late Miocene episodes of connection and isolation in the Mediterranean-Paratethyan realm using Sr isotopes. Sediment Geol 188–189,189–203

Fournier D (1980) Phosphates et pétroles en Tunisie. Géologie comparée des gisements de phosphates et de pétroles. BRGM 24:157–166

Frank M (2002) Radiogenic isotopes. Tracers of past ocean circulation and erosional input. Rev Geophys 40:1–38

Galfati I, Sassi AB, Zaier A, Bouchardon JL, Bilal E, Joron JL, Sassi S (2010) Geochemistry and mineralogy of Paleocene-Eocene Oum El Khecheb phosphorites (Gafsa-Metlaoui Basin) Tunisia. Geochem J 44:189–210

Goldstein SJ, Jacobsen SB (1987) The Nd and Sr isotopic systematics of river-water dissolved material: implication for the sources of Nd and Sr in seawater. Chem Geol 66:245–272

Grandjean P, Cappetta H, Michard A, Albarède F (1987) The assessment of REE patterns and $^{143}Nd/^{144}Nd$ ratios in fish remains. Earth Planet Sci Lett 84:181–196

Henchiri M (2007) Sedimentation, depositional environment and diagenesis of Eocene biosiliceous deposits in Gafsa basin (southern Tunisia). J Afr Earth Sci 49:187–200

Hodell DL, Mueller PA, Garrido JR (1991) Variations in the strontium isotopic composition of seawater during the Neogene. Geology 19:24–27

Hodell DA, Kamenov GD, Hathorne EC, Zachos JC, Röhl U, Westerhold T (2007) Variations in the strontium isotope composition of seawater during the Paleocene and early Eocene from ODP Leg 208 (Walvis Ridge). Geochem Geophys Geosyst 8:Q09001. doi:10.1029/2007GC001607

Huh Y, Tsoi MY, Zaitsev A, Edmond JM (1998) The fluvial geochemistry of the rivers of Eastern Siberia: I. Tributaries of the Lena River draining the sedimentary platform of the Siberian Craton. Geochim Cosmochim Acta 62:1657–1676

Ingram BL (1995) High-resolution dating of deep-sea clays using Sr isotopes in fossil fish teeth. Earth Planet Sci Lett 134:545–555

Jacobsen SB, Wasserburg GJ (1980) Sm–Nd isotopic evolution of chondrites. Earth Planet Sci Lett 50:139–155

Jallouli C, Chikhaoui M, Braham A, Turki MM, Mickus K, Benassi R (2005) Evidence for Triassic salt domes in the Tunisian Atlas from gravity and geological data. Tectonophysics 396:209–225

Keller G, Adatte T, Stinnesbeck W, Stoben D, Kramar U, Berner Z, Li L, von Salis Perch-Nielsen K (1998) The Cretaceous-Tertiary transition on the shallow Saharan platform of Southern Tunisia. Geobios 30:951–975

Kennett JP, Stott LD (1991) Abrupt deep-sea warming, palaeoceanographic changes and benthic extinctions at the end of the Palaeocene. Nature 353:225–229

Koch PL, Tuross N, Fogel ML (1997) The effects of sample treatment and diagenesis on the isotopic integrity of carbonate in biogenic hydroxylapatite. J Archaeol Sci 24:417–429

Kocsis L, Vennemann TW, Fontignie D (2007) Migration of sharks into freshwater systems during the Miocene and implications for Alpine paleoelevation. Geology 35:451–454

Kocsis L, Vennemann TW, Hegner E, Fontignie D, Tütken T (2009) Constraints on Miocene oceanography and climate in the Western and Central Paratethys: O-, Sr-, and Nd-isotope compositions of marine fish and mammal remains. Palaeogeogr Palaeoclimatol Palaeoecol 271:117–129

Koepnick RB, Burke WH, Denison RE, Hetherington EA, Nelson HF, Otto JB, Waite LE (1985) Construction of the seawater curve for the Cenozoic and Cretaceous: supporting data. Chem Geol 58:55–81

Kohn JM, Cerling ET (2002) Stable isotope compositions of biological apatite. In: Kohn JM, Rakovan J, Hughes JM (eds) Review in mineralogy and geochemistry, vol 48. Mineralogical Society of America, Washington, pp 455–488

Kolodny Y, Luz B, Navon O (1983) Oxygen isotope variations in phosphate of biogenic apatites, I. Fish bone apatite-rechecking the rules of the game. Earth Planet Sci Lett 64:398–404

Lazzez M, Zouaghi T, Ben Youssef M (2008) Austrian phase on the northern African margin inferred from sequence stratigraphy and sedimentary records in southern Tunisia (Chotts and Djeffara areas). CR Geosci 340:543–552

Lear HC, Elderfield P, Wilson PA (2000) Cenozoic Deep-Sea Temperatures and Global Ice Volumes from Mg/Ca in Benthic Foraminiferal Calcite. Science 287:269–272

Lécuyer C, Reynard B, Grandjean P (2004) Rare earth element evolution of Phanerozoic seawater recorded in biogenic apatites. Chem Geol 204:63–102

Longinelli A, Nuti S (1973) Oxygen isotope measurements from fish teeth and bones. Earth Planet Sci Lett 20:373–376

Mabrouk A, Belayouni H, Jarvis I, Moody RTJ (2006) Strontium, $\delta^{18}O$ and $\delta^{13}C$ as palaeo-indicators of unconformities: case of the Aleg and Abiod formations (Upper Cretaceous) in the Miskar Field, southeastern Tunisia. Geochem J 40:405–424

Martin EE, Haley BA (2000) Fossil fish teeth as proxies for seawater Sr and Nd isotopes. Geochim Cosmochim Acta 64:835–847

Martin EE, Scher HD (2004) Preservation of seawater Sr and Nd isotopes in fossil fish teeth: bad news and good new. Earth Planet Sci Lett 220:25–39

McArthur JM, Howarth RJ (2004) Strontium isotope stratigraphy. In: Gradstein et al (eds) A geologic time scale. Cambridge University Press, Cambridge, pp 96–105

McArthur JM, Howarth RJ, Bailey TR (2001) Strontium isotope stratigraphy: LOWESS version 3: best fit to the marine Sr-isotope curve for 0–509 Ma and accompanying look-up table for deriving numerical age. J Geol 109:155–170

Miller KG, Kominz MA, Browning JV, Wright JD, Mountain GS, Katz ME, Sugarman PJ, Cramer BS, Christie-Blick N, Pekar SF (2005) The Phanerozoic record of global sea-level change. Science 312:1293–1298

O'Neil JR, Roe LJ, Reinhard E, Blake RE (1994) A rapid and precise method of oxygen isotope analysis of biogenic phosphate. Isr J Earth-Sci 43:203–212

Ounis A (2011) Apport de la géochimie des Terres Rares et des isotopes pour la compréhension des mécanismes de la phosphatogenèse: exemple de la partie occidentale du bassin de Gafsa-Métlaoui. PhD Thesis, University El Manar, Tunis, p 198

Ounis A, Kocsis L, Chaabani F, Pfeifer H-R (2008) Rare earth element and stable isotope geochemistry ($\delta^{13}C$ and $\delta^{18}O$) of phosphorite deposits in the Gafsa Basin, Tunisia. Palaeogeogr Palaeoclimatol Palaeoecol 268:1–18

Palmer MR, Edmond JM (1989) The strontium budget of the modern ocean. Earth Planet Sci Lett 92:11–26

Palmer MR, Edmond JM (1992) Controls over the strontium isotope composition of river water. Geochim Cosmochim Acta 56:2099–2111

Palmer MR, Elderfield H (1985) Variations in the Nd isotopic composition of foraminifera from Atlantic Ocean sediments. Earth Planet Sci Lett 73:299–305

Pearson PN, Palmer MR (2000) Atmospheric carbon dioxide concentrations over the past 60 million years. Nature 406:695–699

Pervinquière L (1903) Étude géologique de la Tunisie centrale. FR de Rudeval, Paris, pp 359

Piepgras DJ, Wasserburg GJ (1980) Neodymium isotopic variations in seawater. Earth Planet Sci Lett 50:128–138

Prokoph A, Shields GA, Veizer J (2008) Compilation and time-series analysis of a marine carbonate $\delta^{18}O$, $\delta^{13}C$, $^{87}Sr/^{86}Sr$ and $\delta^{34}S$ database through Earth history. Earth Sci Rev 87:113–133

Pucéat E, Lécuyer C, Reisberg L (2005) Neodymium isotope evolution of NW Tethyan upper ocean waters throughout the Cretaceous. Earth Planet Sci Lett 236:705–720

Pucéat E, Joachimski MM, Bouilloux A, Monna F, Bonin A, Motreuil S, Morinière P, Hénard S, Mourin J, Dera G, Quesne D (2010) Revised phosphate–water fractionation equation reassessing paleotemperatures derived from biogenic apatite. Earth Planet Sci Lett 298:135–142

Ragaya K, Laatar S, Chouachi A (1991) Carte géologique de Métlaoui au 1/100000. Office de Cartographie et Topographie, Tunis

Sassi S (1974) La sédimentation phosphatée au Paléocène dans le Sud et le Centre Ouest de la Tunisie. Thèse Doct. ès-Sci. Univ. Paris-Sud Orsay, France

Scher HD, Martin EE (2006) Timing and climatic consequences of the opening of Drake Passage. Science 312:428–430

Schmitz B, Ingram LS, Dockery TD, Aberg G (1997) Testing $^{87}Sr/^{86}Sr$ as a paleosalinity indicator on mixed marine, brackish-water and terrestrial vertebrate skeletal apatite in late Paleocene-early Eocene near-coastal sediments, Mississippi. Chem Geol 140:275–287

Sluijs A, Schouten S, Pagani M, Woltering M, Brinkhuis H, Sinninghe Damsté JS, Dickens GR, Huber M, Reichart G-J, Stein R, Matthiessen J, Lourens LJ, Pedentchouk N, Backman J, Moran K, The Expedition 302 Scientist (2006) Subtropical Arctic Ocean temperatures during the Palaeocene/Eocene thermal maximum. Nature 441:610–613

Soudry D, Glenn CR, Nathan Y, Segal I, VonderHaar D (2006) Evolution of Tethyan phosphogenesis along the northern edges of the Arabian African shield during the Cretaceous Eocene as deduced from temporal variations of Ca and Nd isotopes and rates of P accumulation. Earth Sci Rev 78:27–57

Staudigel H, Doyle P, Zindler A (1985) Sr and Nd isotope systematics in fish teeth. Earth Planet Sci Lett 76:45–56

Stille P, Steinmann M, Riggs RS (1996) Nd isotope evidence for the evolution of the paleocurrents in the Atlantic and Tethys Oceans during the past 180 Ma. Earth Planet Sci Lett 144:9–19

Tanaka T, Togashi S, Kamioka H, Amakawa H, Kagami H, Hamamoto T, Yuhara M, Orihashi Y, Yoneda S, Shimizu H, Kunimaru T, Takahashi K, Yanagi T, Nakano T, Fujimaki H, Shinjo R, Asahara Y, Tanimizu M, Dragusanu C (2000) JNdi-1: a neodymium isotopic reference in consistency with La Jolla neodymium. Chem Geol 168:279–281

Thomas P (1885) Sur la découverte de gisements de phosphate du chaux dans le sud de la Tunisie. Comptes rendus de l'Académie des Sciences, Paris 101:1184

Thomas DJ, Bralower TJ, Zachos JC (1999) New evidence for subtropical warming during the late Paleocene thermal maximum: stable isotopes from Deep Sea Drilling Project Site 527, Walvis Ridge. Paleoceanography 14:561–570

Thomas DJ, Bralower TJ, Jones CE (2003) Neodymium isotopic reconstruction of Late Paleocene Early Eocene thermohaline circulation. Earth Planet Sci Lett 209:309–322

Topper RPM, Flecker R, Meijer PTh, Wortel MJR (2011) A box model of the Late Miocene Mediterranean Sea: Implications from combined $^{87}Sr/^{86}Sr$ and salinity data. Paleoceanography 26:PA3223. doi:10.1029/2010PA002063

Trueman NC, Tuross N (2002) Trace elements in recent and fossil bone apatite. In: Kohn JM, Rakovan J, Hughes JM (eds) Review in mineralogy and geochemistry, vol 48. Mineralogical Society of America, Washington, pp 489–521

Vance D, Burton K (1999) Neodymium isotopes in planktonic foraminifera: a record of the response of continental weathering and ocean circulation rates to climate change. Earth Planet Sci Lett 173:365–379

Veizer J, Ala D, Azmy K, Bruckschen P, Buhl D, Bruhn F, Carden GAF, Diener A, Ebneth S, Goddéris Y, Jasper T, Korte C, Pawellek F, Podlaha OG, Strauss H (1999) $^{87}Sr/^{86}Sr$, $\delta^{13}C$ and $\delta^{18}O$ evolution of Phanerozoic seawater. Chem Geol 161:59–88

Vennemann TW, Hegner E (1998) Oxygen, strontium and neodymium isotope composition of shark teeth as a proxy for the palaeoceanography and palaeoclimatology of the northern alpine Paratethys. Palaeogeogr Palaeoclimatol Palaeoecol 142:107–121

Vennemann TW, Fricke HC, Blake RE, O'Neil JR, Colman A (2002) Oxygen isotope analyses of phosphates: a comparison of techniques for analysis of Ag_3PO_4. Chem Geol 185:321–336

Zachos J, Pagani M, Sloan L, Thomas E, Billups K (2001) Trends, rhythms, and aberrations in global climate 65 Ma to present. Science 292:686–693

Zaïer A, Beji-Sassi A, Sassi S, Moody RTJ (1998) Basin evolution and deposition during the Early Paleocene in Tunisia. In: Macgregor DS, Moody RTJ, Clark-Lowes DD (eds) Petroleum geology of North Africa, vol 132. Geol. Soc. London Spec. Publ., pp 375–393

Zili L (2010) Micropaléontologie et biostratigraphie des foraminifères du passage Paléocène-Eocène—Impact du réchauffement climatique global. Thèse Doct ès-Sci, Univ. Tunis El Manar, p 398

Zouaghi T, Bédir M, Inoubli MH (2005) 2D Seismic interpretation of strike-slip faulting, salt tectonics, and Cretaceous unconformities, Atlas Mountains, central Tunisia. J Afr Earth Sc 43:464–486